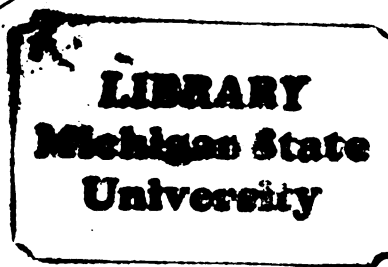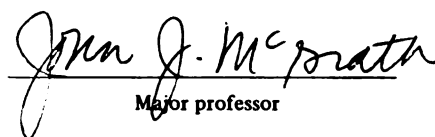This is to certify that the

thesis entitled
CRYOMICROSCOPE INVESTIGATION AND
THERMODYNAMIC MODELING OF THE
FREEZING OF UNFERTILIZED HAMSTER OVA

presented by

Mohsen Shabana

has been accepted towards fulfillment
of the requirements for

M.S. degree in Mechanical Eng.

Major professor

Date 11/10/83

CRYOMICROSCOPE INVESTIGATION AND THERMODYNAMIC MODELING OF THE FREEZING OF UNFERTILIZED HAMSTER OVA

By

Mohsen Shabana

A THESIS

Submitted to
Michigan State University
in partial fulfillment of the requirements
for the degree of

MASTER OF SCIENCE

Department of Mechanical Engineering

1983

ABSTRACT

CRYOMICROSCOPE INVESTIGATION AND
THERMODYNAMIC MODELING OF THE FREEZING
OF UNFERTILIZED HAMSTER OVA

By

Mohsen Shabana

Thermodynamic computer modeling was used to predict the freezing response of single-celled unfertilized hamster ova. The cell membrane transport characteristics were investigated, using a microscope diffusion chamber system. The osmotically-inactive cell volume was experimentally determined to be 21.6% of the initial cell volume. An overall mean value of 0.8 $\mu m^3/\mu m^2 \cdot min \cdot atm \cdot$ ($\equiv 18$ $\mu m/\delta$) was determined for the membrane water permeability L_p. The effect of the extracellular solute concentration on L_p was determined at room temperature ($\sim 23°C$). An existing thermodynamic computer model was used to predict the cell response to freezing. The predicted response was compared to the actual volumetric response observed during freezing on a temperature-controlled cryomicroscope conduction stage. The effect of cooling rate on the nucleation temperature of unprotected ova, and protected ova suspended in a 1.5 M DMSO solution was investigated. Overall mean nucleation temperatures of -13°C and -57.1°C were observed for unprotected and protected ova, respectively.

Finally, cell survival was correlated to the internal ice formation.

بسم الله الرحمن الرحيم

In the name of Allah the most merciful
and the most beneficient

ACKNOWLEDGEMENTS

TABLE OF CONTENTS

LIST OF FIGURES

NOMENCLATURE

A	surface area, cm^3
a	activity
B	cooling rate, $°C/min$
E_a	Activation energy, Kcal/mole
ΔG_{fus}	molar free energy of fusion, Kcal/mole
ΔH_{fus}	latent heat of fusion, Kcal/mole
J	molar flux, $moles/cm^2/sec$
$\tilde{\kappa}$	water conductivity, $\mu m/sec$
L_p	water permeability, $\mu m^3/\mu m^2 \cdot min \cdot atm$
n	number of moles
p	pressure, $dyne/cm^2$
R	gas constant, $dyne \cdot cm/mole \cdot °K$
T	Temperature, $°K$
t	time, sec
V	volume, cm^2
$\bar{v}$	partial molar volume, $cm^3/mole$
x	mole fraction

Subscripts

b	bound
f	final
i	isotonic
J	solute

o	initial
v	volume
w	water

Superscript

i	inside
L	liquid
o	outside
s	solid
*	reference state

Greek

π	osmolality, Osm/kg
μ	chemical potential dyne·cm/mole
ν	dissociation coefficient

CHAPTER 1

INTRODUCTION

1.1   Freezing of Biological Materials

Cryopreservation of biological materials is an area
of growing interest for a variety of people working in
both academic and applied disciplines. Blood and tissue
banking, genetic development of frost-resistent crops,
spermatozoa and ova storage for the purposes of scientific
research, protection of scarce animal species and breeding
of expensive laboratory and domestic animals are among
the numerous advantages of cryopreservation of biomaterials.

In 1949 Polge and colleagues (1) reported a major
breakthrough in cryobiology. They accidentally discovered
that glycerol and propylene glycol protected spermatozoa
against the injurious consequences of exposure to low
subzero temperatures.

Since that time, many workers have succeeded in
freezing different biological materials and for extended
periods of time. Some biomaterials are routinely
cryopreserved with excellent recovery, such as erythrocytes
and lymphocytes. Others are still fragile and yield a low

percentage of survival after thawing, such as human granulocytes.

However, most of the optimal freezing protocols are defined by an entirely empirical approach to the experimental work. This can be attributed to a lack of understanding of the basic mechanisms involved in cell damage during freezing.

A number of theories that describe the cell damage mechanism have been presented most of which lack adequate experimental evidence.

Lovelock (2,3) proposed that the increased concentration of electrolytes in the cell suspension during freezing could break down the membrane components. In addition the dilution of the cell suspension during thawing could produce an osmotic shock that could also damage the cell.

Others proposed that during freezing a certain critical amount of so-called "bound" water is removed from vital cellular components such as membranes and proteins, which causes cell death (4).

Meryman (5) suggested that cell dehydration during freezing, results in a fatal increase in the membrane permeability for normally impermeable solutes.

In 1972 Mazur and co-workers (6) presented their widely accepted theory for cell damage during freezing: the "Two Factor" hypothesis. They related cell damage to two competing phenomena, each dominates a specific range

of cooling rantes. Specifically these phenomena are, "formation of internal ice crystals" at fast cooling rates, and "solution effects" at slow cooling rates.

The schematic in Figure 1 describes Mazur's theory. Figure 1-a shows the effect of intracellular ice formation on cell survival, while Figure 1-b shows the solution effect. The solid line in Figure 1-c represents the proposed cell survival when the two modes of damage are combined. Quantitatively, the experimental observations shown in Figure 2 support Mazur's theory. This figure shows cell survival as a function of cooling rate for a number of different cell types. An optimum cooling rate where cell survival is maximum is observed for each cell type. An apparent decrease in cell survival on both sides of that optimum cooling rate is in strong agreement with the proposed damage theory schematically described in Figure 1-c.

For a better understanding of the two modes of cellular damage, the equilibrium aspects of the freezing process are explained below.

Figure 3 shows the typical elements of a model describing water transport across the cell membrane during freezing. When heat is removed from the system, water starts to solidify in the external medium forming pure ice, where salts are assumed to be rejected from the ice to the liquid water phase. The cell membrane is modeled as a semi-permeable barrier, which prevents the permeation
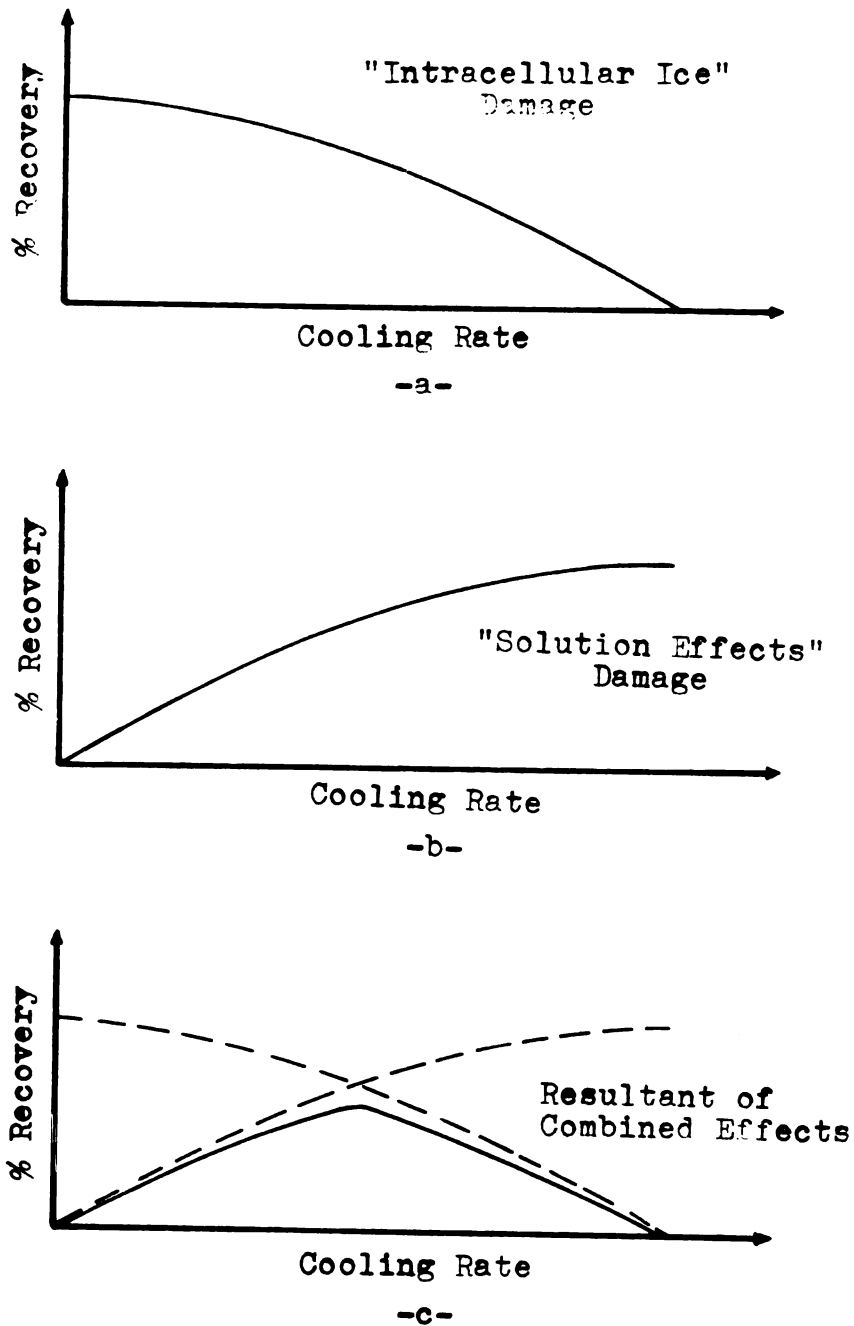
Figure 1. A schematic of the Two-Factor
hypothesis.

(Reproduced from McGrath (8))
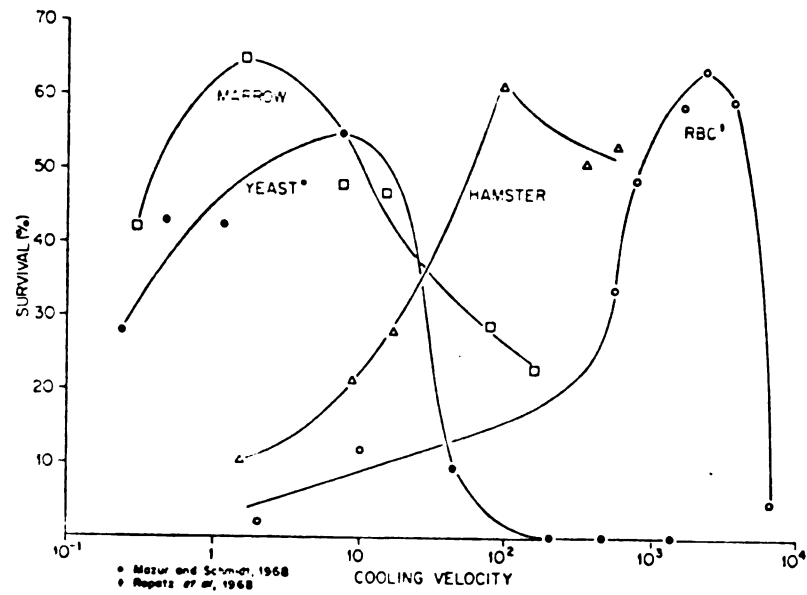
Figure 2. Cell survival as a function
of cooling rate for several
cell types.

(Reproduced from Mazur et al. (7))
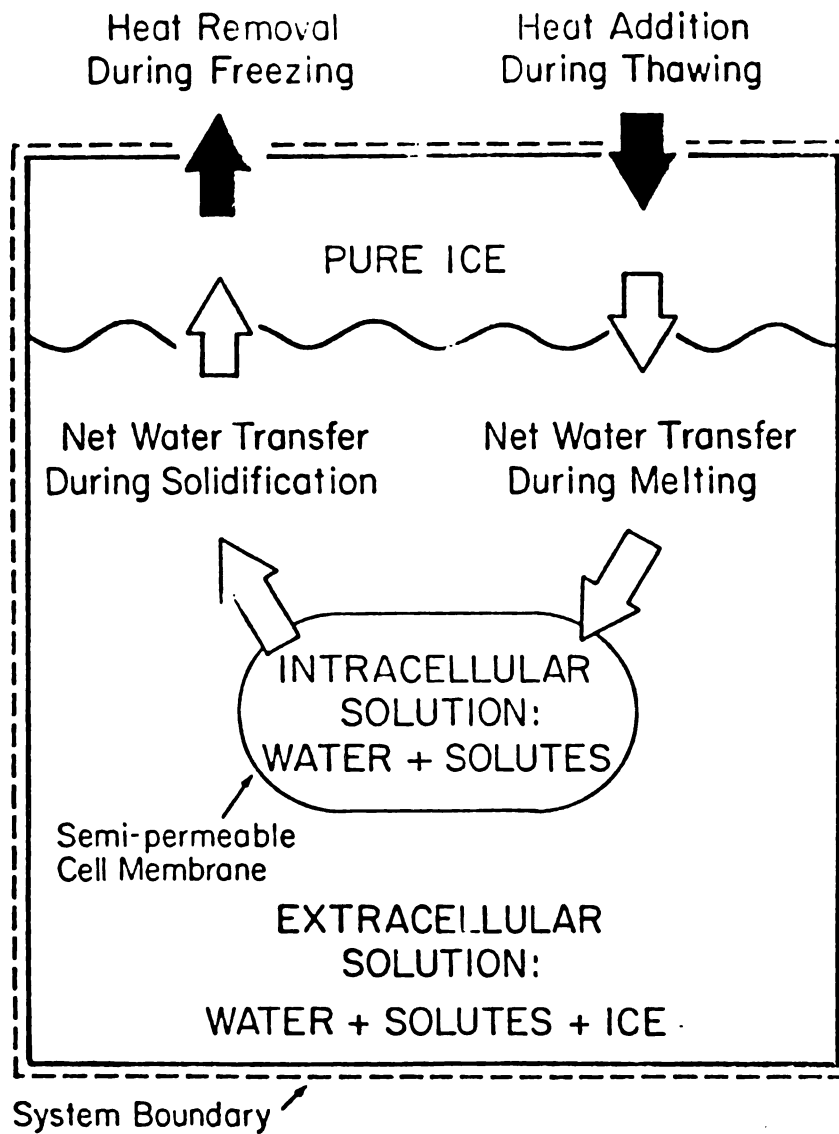
Figure 3. A model describing cell water transport during freezing.

(Reproduced from McGrath (8))

of solutes into the cell. It also prevents the penetration
of the external ice into the cytoplasm, hence preventing
the intracellular water from freezing. Consequently, two
transient events occur. First the chemical potential of
the external water decreases, creating a state of
chemical non-equilibrium across the cell membrane.
Secondly the cell water supercools and becomes more
likely to form ice. For the cell to regain a state of
equilibrium it has to follow one of the two paths described
in Figure 4. During slow cooling, the difference in
chemical potential drives the intracellular water outside
the cell where it freezes externally. A state of
equilibrium is re-established across the cell membrane,
and the cell shrinks due to dehydration. In this case
the process is said to be mass transfer-dominated. The
cell damage in this process is believed to be due to the
so-called "solution effects" which include all of the
various cell damage theories described above.

At fast cooling rates, despite the rapid increase
in water chemical potential gradient across the membrane,
the water does not have enough time to leave the cell.
The cell water becomes more supercooled and forms ice
inside the cell in order to achieve chemical equilibrium
with the external medium. Here, the process is said
to be heat transfer-dominated.

In this case the cell volume change is minimal if
it occurs at all. The cell damage at fast cooling rates
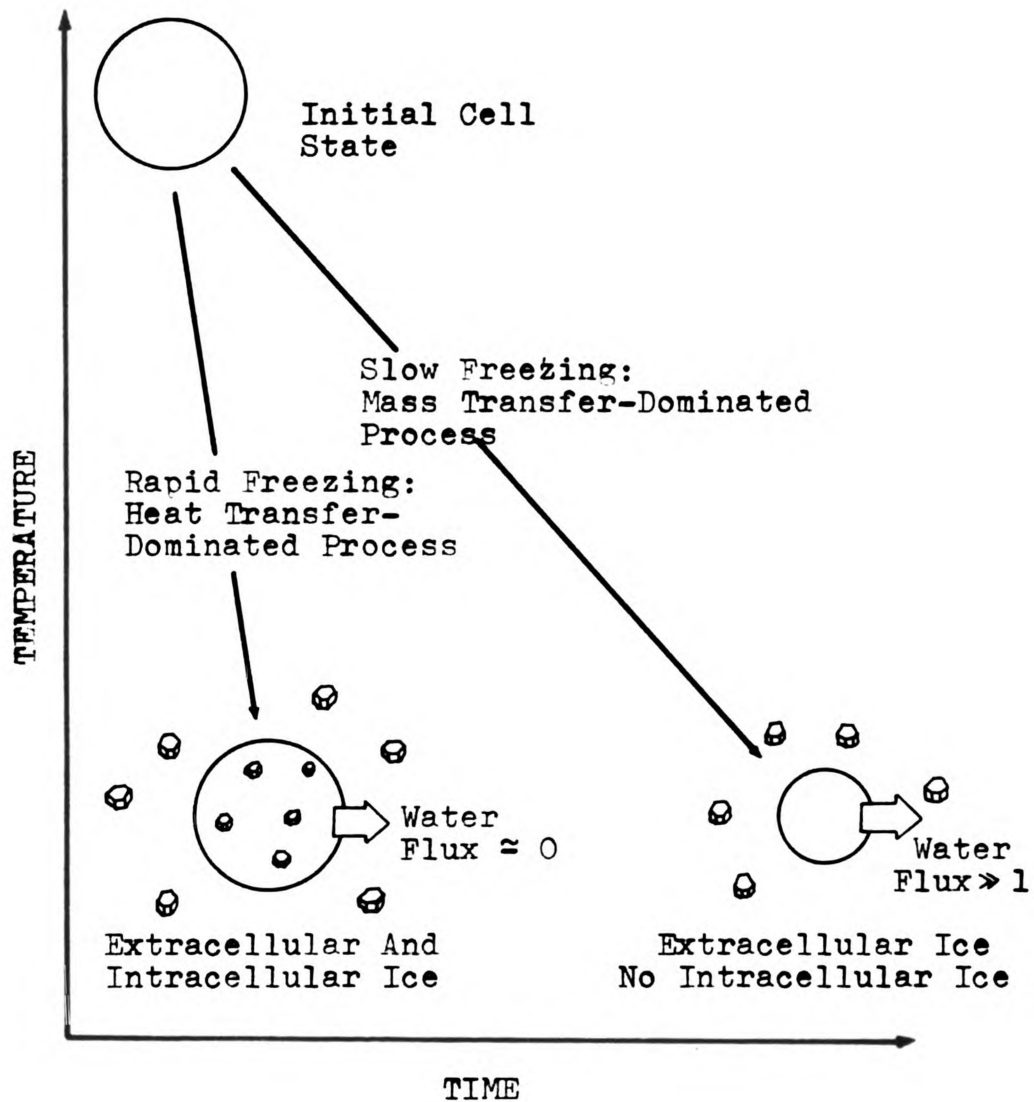
Figure 4. Alternative methods for a suprecooled cell to achieve equilibrium.

(Reproduced from McGrath (8))

is commonly attributed to the mechanical deformation exerted by the intracellular ice crystals on the cell organelles (9).

As the selective barrier between the inside of the cell and the outside suspending medium, the cell membrane is believed to be the primary site of cell damage (2-5). The problem remains unsolved as to whether physical or chemical aspects are responsible for cellular death. However, as described in most theories water transport across the cell membrane and the amount of water remaining within the cell play a highly significant role in cell damage (6). Therefore, the mathematical modeling of the kinetics of water transport across the cell membrane, become a logical and a necessary step in developing an improved understanding of the mechanisms involved.

In 1963 Mazur (10) began a new era in cryobiology. He introduced the first thermodynamic model describing the kinetics of water loss from a cell as a function of various parameters.

Among these parameters, the temperature, the cooling rate, the ratio of cell surface area to volume, the membrane hydraulic permeability and its temperature coefficient were included. However, Mazur's model was based on a number of simplifying assumptions. These assumptions include: modeling the cytoplasm as an ideal dilute solution; no thermal or concentration gradients

were allowed in the cooled cell sample; the membrane was assumed impermeable to solutes and; a state of equilibrium exists between the solid and liquid water phases. These assumptions and others were investigated in subsequent non-equilibrium models (10,11). However the main structure of Mazur's original model remains intact.

A computer simulation of the freezing process based on a thermodynamic model can be used to predict the cell volumetric response to freezing and thawing. The predicted response can then be compared to actual cell behavior obtained from cryomicroscopic experiments.

Such comparisons have been used for two purposes: 1) to assess the validity of the mathematical/thermodynamic model itself and; 2) to investigate the significance of various assumptions and parameters included in the model. However, the real future goal of the modeling process is to be able to predict the response of experimentally untested biological cells. Such predictions are not yet established because of a lack of understanding with respect to the complicated nature of the biological cells.

In order to test the cell response, and experimentally investigate different modeling aspects of the problem, sophisticated equipment is required.

Cryomicroscope systems have been designed and developed in a number of laboratories (12-15). The basic features of such a microscope system are: 1) the ability to cool the cell suspension to low subzero temperatures;

2) the ability to observe the cell sample in real time at accurately measured temperatures and; 3) the ability to control both the temperature and the rate of temperature change (usually linear rates of cooling and warming).

The development and use of such cryomicroscopes has allowed the determination of the likelihood of intracellular ice formation, measurements of cell volume during freezing and thawing, as well as other investigations such as gas bubble formation inside the cell during freezing and thawing (38).

1.2   Ova and Embryo Freezing

Unfertilized and fertilized mouse ova as well as preimplantation-stage embryos have been successfully frozen to -196 or even -296°C. When transferred into foster mothers they yield live pups (16,17). The survival was achieved by slow freezing rates (0.2-2.0°C/min) and moderate warming rates (4-25°C/min). Glycerol and dimethylsulphoxide (DMSO)(mostly the latter) were used as cryoprotective agents to protect the embryos against the deleterious low temperature effects. The same technique was applied in many laboratories to preserve embryos from several other mammals, e.g. cattle, sheep, goats, rabbits and rats (18).

Mammalian embryos have been used for the microsopic investigation of both intracellular nucleation as well as volume changes during freezing and thawing. Their

relatively large size (~10 times the diameter of human erythrocytes) and their spherical shape permit volume changes to be calculated from cross sectional areas.

Several techniques have been reported whereby membrane permeability can be determined from volume measurements performed on single cells.

Liebo (19) evaluated the permeability of mouse ova using the following technique: 1) an ovum was suspended in a vertical column filled with an osmotically active solution; 2) as the ovum changed volume by water flux its density was changed correspondingly; 3) as the density changed the ovum was forced to rise or fall and; 4) the slowly moving ovum was photographed at small time intervals and the transient volumes were recorded. A different technique was used in this thesis. A diffusion chamber (described below) was used to observe the transient cell volumes while changing the concentration of the suspending solution, simultaneously.

Unfertilized, rather than fertilized, hamster ova were used in the present study for convenience because microliter volumes of frozen-thawed samples of ova cannot be quantitatively recovered from the microscope stage. Therefore, further direct analysis of the treated ova, such as *in-vitro* survival assays would not have been possible. However, the effect of fertilization and development on the different parameters involved in the freezing of hamster ova is suggested for future work.

1.3   Goals of the Present Thesis Work

The goals of this work as guided by the techniques and results of previous workers are: 1) to determine the so-called "osmotically-inactive" volume of unfertilized hamster ova; 2) to determine the plasma membrane hydraulic permeability (L_p) of unfertilized hamster ova; 3) to determine the effect of the concentration of the suspending medium on L_p; 4) to use the water permeability obtained in an existing computer model to predict the quantitative cellular response during freezing; 5) to experimentally determine the ova volumetric response during freezing and correlate that response to the model predictions and; 6) to determine the nucleation temperatures of unprotected as well as protected hamster ova suspended in a DMSO solution as a function of the cooling rate. This last factor then determines the effect of DMSO as a cryoprotective agent on the nucleation temperature of unfertilized hamster ova.

CHAPTER 2

THERMODYNAMIC AND MATHEMATICAL MODELING

2.1   Introduction

In 1963 Mazur (20) derived equations to describe the kinetics of water loss from a cell during the freezing process as a function of various parameters. These parameters include: temperature; cooling rate; the cell membrane water permeability; the temperature dependency of the permeability; and the ratio of the cell surface or membrane area to volume. This was the first thermodynamic model delineating the osmotic response of cells to freezing. Since that time a number of quantitative models that share the fundamental framework with Mazur's model (21-24) have been published.

The fundamental reasons for the development of a thermodynamic model are: 1) to predict cell volume during freezing and; 2) to predict the thermodynamic state of the intracellular system. Two expressions, one for the concentration of the intracellular contents as well as one for the extracellular medium as a function of the system temperature are required. The difference between these concentrations represents the thermodynamic potential that drives

14

the water into or out of the cell at any given temperature.
The cell membrane is a selective barrier that controls
the water flux, and which is essential for unequal osmotic
pressures inside and outside the cell to exist. Hence,
both the internal and the external concentration expressions
have to be linked through the transport characteristics
of the cell membrane. The resulting expression is the
thermodynamic model that predicts the amount of water
remaining inside a dehydrating cell during freezing at
any subzero temperature and at any given cooling rate.

A typical model for a biological cell suspended in an
isotonic medium is shown in Figure 3. The model consists
of the following elements: i) The extracellular solution,
consisting of water and solutes; ii) An intracellular
solution of a complicated biological nature that is
simply modeled as water and a single solute; iii) The cell
membrane, which is modeled as a semipermeable membrane
that allows the diffusion of the solvent (water in this
case), but in this model does not allow for the transport
of any solute molecules. In general, this assumption
is not strictly true. However, it is a good approximation
since the permeability of cells to water is several orders
of magnitude higher than to the non-permeating solutes
normally found in protoplasm (20).

For a complete investigation, the water transport
characteristics of the cell membrane must be obtained
either from experimentation or from the literature.

The modeling approach used in this work was developed
and modified by Mazur (20), Levin (21), Mansoori (25),
and other researchers. It has been developed in the
present laboratory by Callow (26).

2.2   The Extracellular Solution

It is assumed that the external solution behaves as
an ideal solution. Hence, a relationship between the
water mole fraction outside the cell and the temperature
of the system which is assumed to be uniform (25) can
be developed from the basic equation for the chemical
potential of an ideal solution:

$$\mu_w^L(T,p,x) = \mu_w^{L,*}(T,p) + RT \ln x_w \qquad (2\text{-}1)$$

where, $\mu_w^{L,*}$ is the chemical potential of pure liquid water,
used as a reference value, x_w is the water mole fraction,
and RT and p have their usual meaning.

Assuming that the solid/liquid water phases are
in a state of mutual equilibrium, an equality holds for
the chemical potentials of water in both phases (27),

$$\mu_w^L(T,p,x) = \mu_w^S(T,p) \qquad (2\text{-}2)$$

where, μ_w^L and μ_w^S are the chemical potentials of liquid
water in solution and pure solid water, respectively.
The above expression includes the assumption that all
the solutes in the solution are rejected from the solid
phase to the liquid water phase. In other words, the

solid phase is assumed to be pure water. Substituting Equation (2-1) into Equation (2-2) yields

$$\ln x_w = -\left[\frac{\mu_w^S(T,P) - \mu_w^{L,*}(T,p)}{RT}\right] \qquad (2\text{-}3)$$

and substituting the following expression,

$$\Delta G_{fus} = \mu_w^S(T,p) - \mu_w^{L,*}(T,P)$$

where ΔG_{fus} is the molar free energy of fusion of pure water at temperature T (27), into Equation (2-3) results in,

$$\ln x_w = \frac{-\Delta G_{fus}}{RT} \qquad (2\text{-}4)$$

Equation (2-4) can be differentiated with respect to X at constant pressure. Using the Gibbs-Helmholtz expression,

$$\left[\frac{\partial(\Delta G/T)}{\partial T}\right]_p = -\frac{\Delta H}{T^2} \qquad (2\text{-}5)$$

Equation (2-4) becomes,

$$\frac{1}{x} = -\frac{\Delta H_{fus}}{RT^2}\left(\frac{\partial T}{\partial x}\right)_p \qquad (2\text{-}6)$$

where, ΔH_{fus} is the latent heat of fusion of pure water.

Integrating Equation (2-6),

$$\int_{x_w}^{x}\frac{dx}{x} = \int_{T_o}^{T}\frac{\Delta H_{fus}}{RT^2}\,dT \qquad (2\text{-}7)$$

where, the lower limit corresponds to pure water, for which the mole fraction $x_w = 1$, and T_o is the freezing temperature. The upper limit corresponds to the mole fraction at any prescribed subzero temperature. Also assuming that ΔH_{fus} is independent of temperature over the experimental temperature range, Equation (2-7) yields,

$$\ln x_w = \frac{\Delta H_{fus}}{R}\left(\frac{1}{T_o} - \frac{1}{T}\right) \qquad (2\text{-}8)$$

Equation (2-8) describes the concentration of the solute in the extracellular solution as a function of the temperature of the system. Also, from the assumption of ideality made above, it is true that the water activity outside the cell, a_w^o, is identical to the water mole fraction x_w^o. Thus:

$$\ln a_w^o = \frac{\Delta H_{fus}}{R}\left(\frac{1}{T_o} - \frac{1}{T}\right) \qquad (2\text{-}9)$$

Equation (2-9) describes the extracellular water activity as a function of the uniform system temperature.

2.3   The Intracellular Solution

The mole fraction of water inside the cell can be described by the formula,

$$x_w^i = \frac{n_w^i}{n_w^i + \sum_j \nu_j n_j^i} \qquad (2\text{-}10)$$

where, $n_w^i \equiv$ number of water molecules inside the cell,

$n_j^i \equiv$ number of molecules of the jth solute inside the cell

and $\nu_j \equiv$ the dissociation coefficient of the jth solute

species.

However, due to the complicated nature of the internal

solution of most biological cells including the ova used

here, and the lack of detailed information about their

constituents, it is virtually impossible to calculate the

internal water mole fraction by means of Equation (2-10).

Instead, for a state of chemical equilibrium to exist

across the cell membrane, the initial mole fraction of the

intracellular water is considered to be equal to that

of the extracellular isotonic solution in which the ova

naturally exist. Using the water transport equations,

the number of moles of water leaving the cell as the

system temperature is lowered can be calculated. Finally,

if it is assumed that the cell membrane is semipermeable

(i.e. no solute molecules can pass across it in either

direction), the instantaneous mole fraction of water

inside the cell can be calculated.

The intracellular solution is modeled as an ideal

solution (20), for which the water activity is equal to

its mole fraction,

$$x_w^i = a_w^i \qquad\qquad (2-11)$$

where, x_w^i and a_w^i are the water mole fraction and activity

inside the cell, respectively.

Equations (2-9), (2-11) and the membrane transport characteristics are essential for the calculation of the rate of water flow across the cell membrane as a function of temperature.

2.4   Water Transport Model

Levin (21) described the water flux across the cell membrane as a function of the chemical potential gradient by,

$$\left. J_w \right)_{out} = \frac{-1}{A} \frac{dn_w^i}{dt} = \frac{L_p}{\overline{v}_w^2} (\mu_w^i - \mu_w^o) \tag{2-12}$$

where, J_w is the water mole flux, A is the membrane surface area, t is time and L_p is the membrane hydraulic water permeability expressed in (cm^3/dyn·sec) or ($\mu m^3/\mu m^2$·min·atm).

The water chemical potential is given in the form (28),

$$\mu_w = \mu_w^*(T) + \overline{v}_w p + RT \ln a_w \tag{2-13}$$

where, μ_w^* is a reference chemical potential, $\overline{v}_w$ is the molar volume of water and p is the pressure. Neglecting the hydrostatic pressure gradient across the cell membrane (23), Equations (2-12) and (2-13) result in,

$$\frac{dn_w}{dt} = \frac{\tilde{\kappa} \cdot A}{\overline{v}_w} (\ln a_w^i - \ln a_w^o) \tag{2-14}$$

where, $\tilde{\kappa}$ is the membrane water conductivity (μm/sec)

or

w

w

s

a

w

a

a

a

w

ar

$$\tilde{\kappa} = L_p \frac{RT}{\bar{v}_w}$$

or,

$$\frac{dn_w}{dT} = \frac{\tilde{\kappa} \cdot A}{\bar{v}_w \cdot B} (\ln a_w^i - \ln a_w^o) \tag{2-15}$$

where the cooling rate, B, is given as

$$B = \frac{dT}{dt} \tag{2-16}$$

Equation (2-15) relates the outward mole flux of water across the cell membrane as a function of the uniform subzero temperature to the natural logarithm of the water activity on both sides of the membrane. To perform a computer simulation for the cell dehydration during freezing using Equation (2-15), the membrane water permeability (L_p) has to be obtained.

2.5   Membrane Water Permeability

Terwilliger and Solomon (29) described the bulk volume flow of water, J_v, across the cell membrane, in a state of chemical potential non-equilibrium and in the absence of a transmembrane hydrostatic pressure difference as,

$$J_v = RT L_p (\Pi_{in} - \Pi_{out}) \tag{2-17}$$

where, Π_{in}, Π_{out} denote the osmolality of intracellular and extracellular solutions respectively.

effe

cons

(2-

whe

and

wh

th

eq

$V($

th

and

are

cal

V_b.

soli

boun

memb

Assuming that the water permeability, L_p, the effective membrane area, and the temperature T remain constant during the course of an experiment, Equation (2-17) can be integrated to produce:

$$\beta t \cdot L_p = \bar{v} \left(\frac{\Pi_f}{\Pi_i} - 1 \right) - \ln \left(1 - \bar{v} \right) \qquad (2\text{-}18a)$$

where,

$$\beta = \frac{A \, RT \, (\Pi_f)^2}{(V_i - v_b) \Pi_i} \qquad (2\text{-}18b)$$

and,

$$\bar{V} = \frac{V(t) - V_i}{V_f - V_i} \qquad (2\text{-}18c)$$

where, V_b is the osmotically inactive cell volume, V_i is the isotonic cell volume, V_f is the final or the equilibrium cell volume in the non-isotonic solution, $V(t)$ is the cell volume at time t, (cm^3), Π_i and Π_f are the osmolalities of the extracellular solution before and after mixing (osm/cm^3), A is the membrane surface area (cm^2), and R is the gas constant $(dyn \cdot cm/mole \cdot °k)$.

An important parameter that is required for the calculation of L_p is the osmatically inactive cell volume V_b. That volume can be described as the volume of the solid material plus the volume of water (within the cell boundary) that is not free to move across the cell membrane in response to an osmotic gradient (37).

This parameter was obtained experimentally utilizing the so-called Boyle-Van't Hoff plot (which will be discussed in Chapter 4).

A number of **researchers** (20,21) described the temperature dependence of L_p as:

$$L_p = L_p \Big)_{T_g} \exp\left[-\frac{E_a}{R}\left(\frac{1}{T} - \frac{1}{T_g}\right)\right] \tag{2-19}$$

where, $L_p \Big)_{T_g}$ corresponds to the water permeability at $T_g = 293.15°K$, and E_a is the apparent activation energy for the permeation process.

However, Levin (30) mentioned that the above equation can be applied only to the simplest types of membrane systems. For more complicated membrane systems (i.e. a number of parallel membranes resisting the water flow), one may require a more complicated expression for temperature and/or solute concentration dependence for the overall cell water permeability.

Diller and Bradley (31) proposed two possibilities for the dependence of L_p on the solute concentration. The first one is an exponential relation expressed in the form,

$$L_p = L_p \Big)_{T_g} \exp\left[\frac{E_a}{R}\left(\frac{1}{T_g} - \frac{1}{T}\right) + E_c\left(\frac{1}{\Pi} - \frac{1}{\Pi_g}\right)\right] \tag{2-20}$$

while the second relation shows a linear dependence of the form,

$$L_p = L_p\Big)_{T_g} \left[\exp\left[\frac{E_a}{R}\left(\frac{1}{T_g} - \frac{1}{T} \right) \right] + E_c\left(\frac{1}{\Pi} - \frac{1}{\Pi_g} \right) \right] \qquad (2\text{-}21)$$

where, the first part of the right-hand-side of Equations (2-20) and (2-21) is the temperature dependence shown in Equation (2-19). E_c is the permeability concentration coefficient and Π_g is the reference solute concentration at the reference temperature T_g. Scheiwe et al. (32,33) have used another form of equation:

$$L_p = L_p\Big)_{T_g} \exp\left[b\left(1 + a_2\, \frac{\Pi - \Pi_g}{\Pi_g}\right)\left(T - T_g\right) + a_1\left(\frac{1}{\Pi} - \frac{1}{\Pi_g} \right) \right]$$

$$(2\text{-}22)$$

where, a_1 and a_2 and b are coefficients of the L_p function.

A discussion of the effect of temperature and solute concentration on L_p for hamster ova is presented in Chpater 4 of this thesis.

In summary, cell volume changes during freezing are determined numerically from:

$$V = V_o - \bar{v}_w \int_{T_o}^{T} \frac{dn_w}{dT}\, dT \qquad (2\text{-}23)$$

where, V_o is the initial cell volume at the freezing temperature T_o ($^\circ$K), and $\bar{v}_w$ and n_w are the apparent molar volume and the number of moles of water, respectively, where:

$$\frac{dn_w}{dT} = \frac{\tilde{k} \cdot A}{\bar{v}_w \cdot B}\, (\ln a_w^i - \ln a_w^o) \qquad (2\text{-}15)$$

where, A is the membrane surface area, B is the cooling rate ($^\circ$C/min), and a_w^i and a_w^o are the water activity inside and outside the cell, respectively. $\tilde{\kappa}$ is the membrane hydraulic conductivity (μm/sec) and is equal to

$$\tilde{\kappa} = L_p \frac{RT}{\overline{v}_w}$$

where L_p is the membrane water permeability obtained from experiments, by means of Equation (2-18) described above. The temperature dependence of L_p is in the form

$$L_p = L_p \Big)_{T_g} \exp\left[-\frac{E_a}{R}\left(\frac{1}{T} - \frac{1}{T_g}\right)\right] \qquad (2\text{-}19)$$

where L_p corresponds to the water permeability L_p at $T_g = 293.15^\circ$K. The activation energy, E_a, in Equation (2-19) has been determined from the literature (19). The concentration dependence of L_p described in Equations (2-20) through (2-22) has been assumed insignificant due to experimental results to be described in Chapter 4 in this thesis. The cell membrane is assumed semi-permeable. The membrane surface is assumed to be that of a shrinking sphere. No concentration or thermal gradients are assumed to exist within the cell sample as well as the cell itself. Hydrostatic pressure gradients across the membrane are neglected. These simplifying assumptions and others are discussed in detail in Chapter 4 of this document.

CHAPTER 3

EXPERIMENTAL TECHNIQUES

3.1   Cell Sample Preparation

Hamster ova were obtained by the method described
by DeMayo (1). Hamsters were induced to superovulate
by an intraperitonial (IP) injection of 30 IU pregnant
mare serum (PMS, Folligon^R; Intervet Laboratories;
Bar Hill, Cambridge, Great Britain) between 900 hrs and
1200 hrs of age followed 56 to 64 hrs later with an IP
injection of 30 IU human choronic gonadotropin, HCG
(APL^R; Ayerst Laboratories Inc., NY). The hamsters were
sacrificed by cervical dislocation, 14 to 16 hrs after
HCG administration. The oviducts were removed, dissected
free of fat and flushed from the fimbrie with 0.3 ml of
either Dulbeccos phosphate buffered saline (PBS) (Gibco
Laboratories, Grand Island, NY) or a modification of the
squirrel monkey *in-vitro* fertilization medium used by
Kuehl and Dukelow (1979), TC-199. Cumulous cells were
removed by an addition of 1 mg/ml of hyaluronidase
(Sigma Corp., St. Louis, MO) to the collection medium.
Fresh cells were then washed in 0.3 ml of medium and
held in an ice bath for no longer than 3 hrs until

26

transferred to either the diffusion chamber or the cryomicroscope stage (both described below).

Cryoprotectant: For the experiments that required the addition of a cryoprotective agent, 0.2 ml of a 3 M dimethylsulfoxide solution (DMSO; Baker Chemical Co., Phillipsburg, PA) were added to an equal volume of cell medium for a final concentration of 1.5 M solution. Healthy cells (75 to 80 μm dia.) were transferred to the mixture at room temperature (23°C), where they were held on ice for at least 10 minutes, allowing them enough time to equilibrate with the 1.5 M solution before the transfer to the experimental apparatus.

3.2   The Diffusion Chamber System

Figures 5a and 5b show a schematic of the diffusion chamber designed by Ligon (35). The system consists of two compartments separated by a dialysis membrane. A drop of cell suspension is held stagnant in the upper compartment. The lower compartment is initially filled with a solution isotonic with the cell suspension. The volume of the lower compartment is extremely large compared to that of the upper compartment. Hence, the lower compartment can be considered as an infinite reservoir. This allows the extracellular solution in the upper sample space to attain a final equilibrium concentration equal to that of the bulk solution in the lower compartment. At time equal to zero the lower
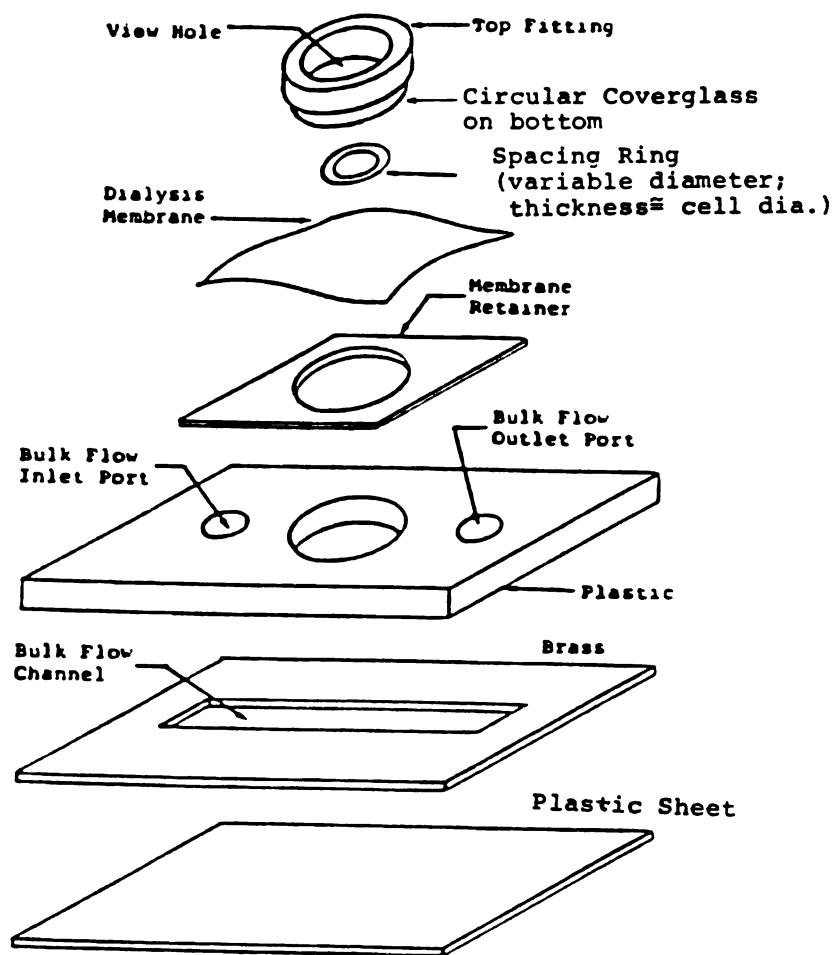
Figure 5a. Exploded view of the diffusion chamber.

(Reproduced from Nowlen(35))
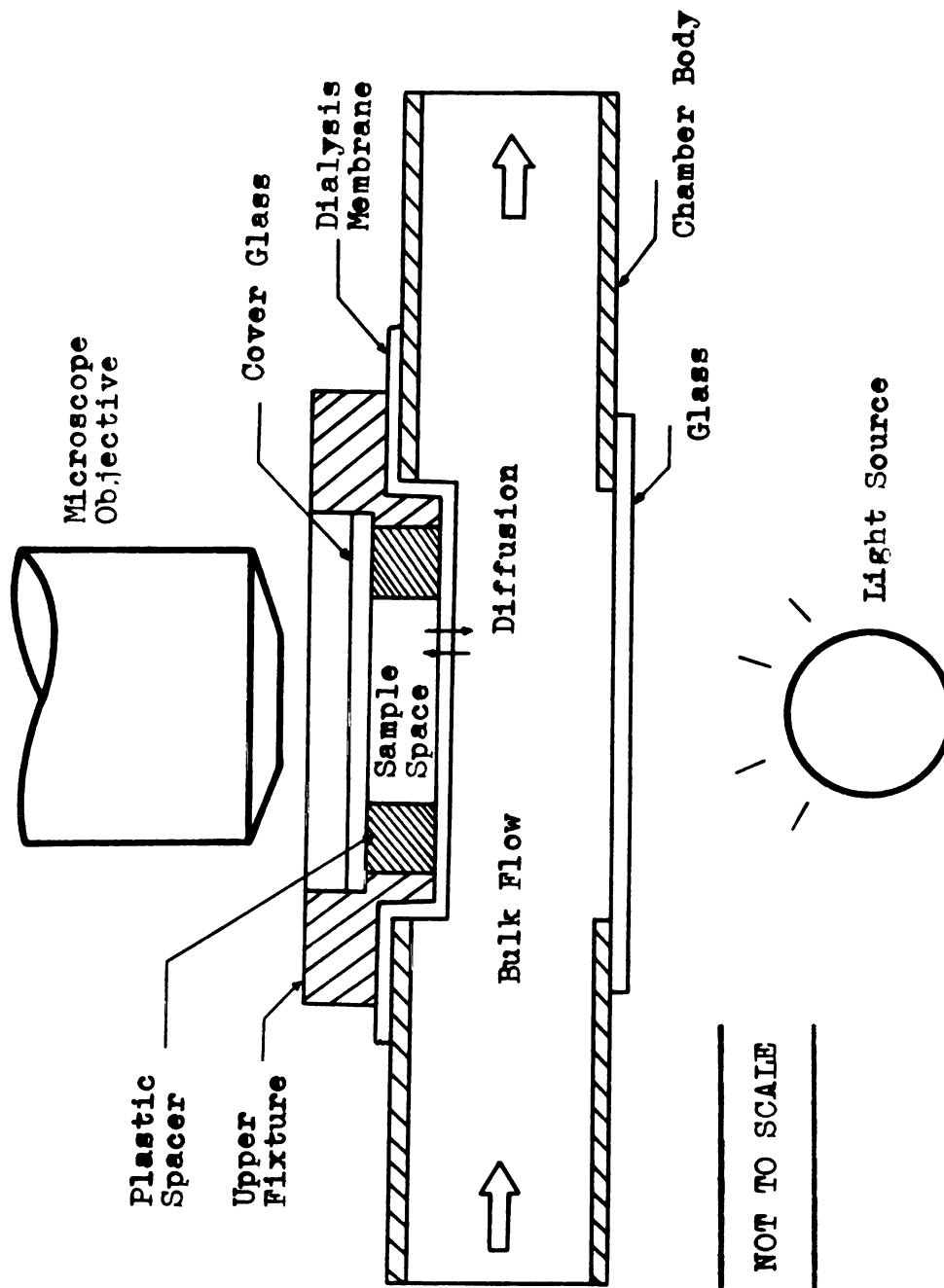
Figure 5b. Schematic of the Diffusion Chamber

NOT TO SCALE

compartment is flushed with a new solution whose concentration is either hypotonic or hypertonic with respect to the cell suspension. If the solution in the lower compartment has a concentration higher than that of the cell suspension in the upper compartment, solutes will diffuse upward across the dialysis membrane from the lower to the upper compartment and *vice versa*.

As shown in Figure 5c, two pressurized bottles (1000 cc) are connected to two small single pumps. The outlet of each pump is connected with plastic tubing to the inlet ports of a two-way switch. The outlet of the switch is connected with plastic tubing to the inlet at the lower compartment of the diffusion chamber. The outlet of the lower compartment is connected to a discharge container. The entire mechanism is used to regulate the bulk flow in the lower compartment. It is also used to facilitate changing the osmolality of the bulk flow from isotonic to non-isotonic and *vice versa*. This will in turn change the osmolality of the extracellular solution in the upper compartment. The system can be modified to include more solution bottles.

Once the lower compartment is filled with a non-isotonic solution, e.g. hypertonic, the solutes will gradually diffuse across the dialysis membrane to the upper sample region. Consequently, the concentration of the solution in the upper compartment will increase in some fashion. A certain amount of time will elapse until a state of transmembrane chemical equilibrium is
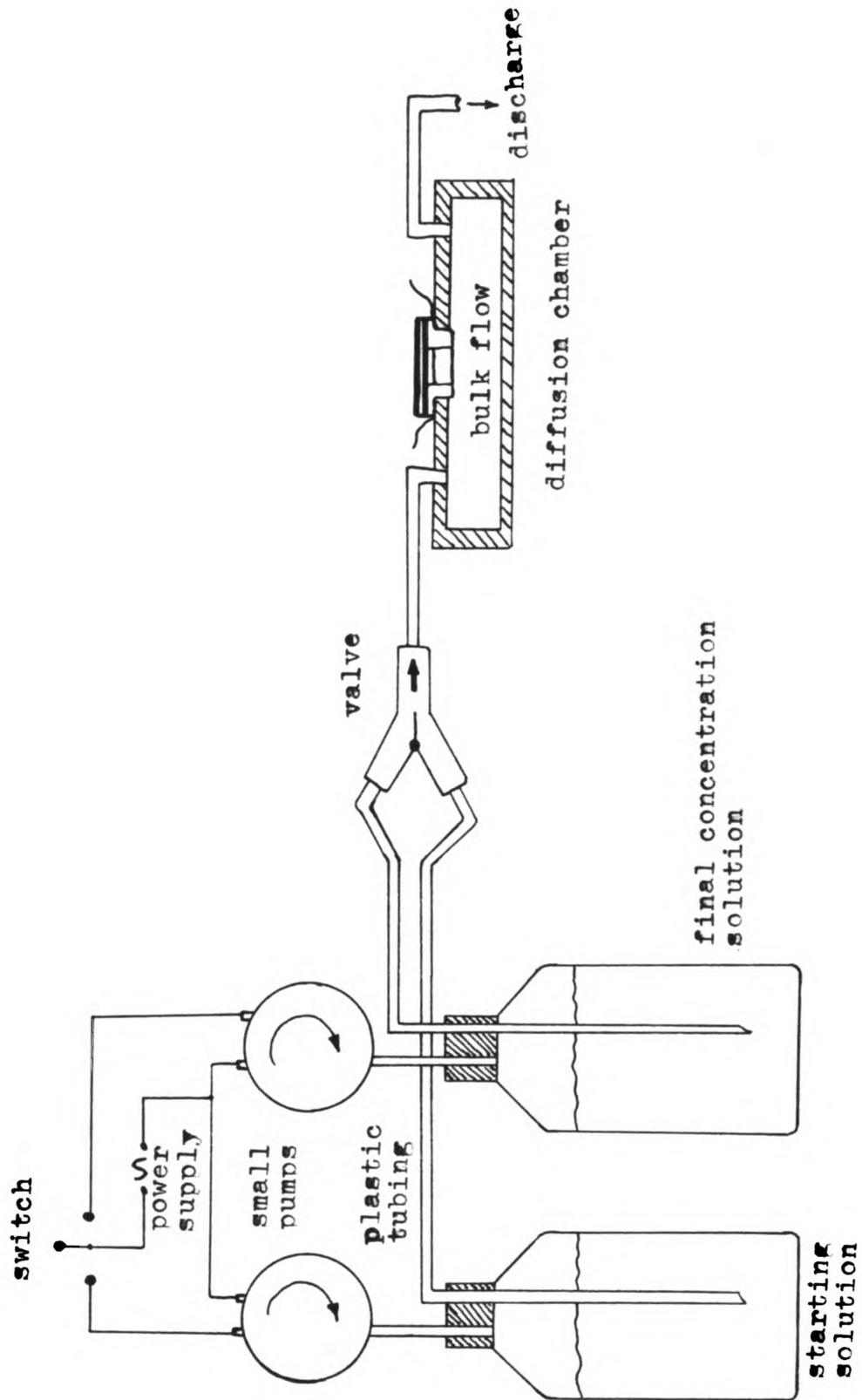
Figure 5c. Layout of the diffusion chamber connected to the flushing mechanism.

established. This time constant will depend primarily on the transport characteristics of the dialysis membrane for each of the solutes present.

Preliminary analytical studies by Ligon (35) suggested that for NaCl, a typical solute of interest, the sample region will have negligible concentration gradients. Hence it can be characterized by a single concentration. Ligon could also show, both analytically and optically, that the time constant required for the solution in the sample region to equilibrate with that in the lower compartment ranges from 3 to 6 seconds.

Nowlen (36) assumed that concentration gradients within the sample compartment are negligible and concluded from a simple analytical model that the concentration of the solute in the sample region is expressed as an exponential function of various parameters. These parameters are: the concentration of the bulk solution; the initial concentration of the sample region; the permeability of the dialysis membrane to that solute; the volume of the sample region; the effective area of dialysis membrane available for transfer, and time.

Nowlen found that using a Cuprophan 80 pm dialysis membrane and a sodium chloride solution, the time delay is approximately 59 seconds for 95% response time. This is a significantly long time compared to the 3-4 minute period during which the hamster ova were observed to shrink.

The major difference between Ligon's case and Nowlen's was the fact that Ligon's model was for a chamber thickness of 12 μm whereas Nowlen's model was for a chamber thickness of approximately 250 μm.

Experimental results of the present work, using hypertonic NaCl solutions and a Cuprophan 80 m membrane (Membrana GmbH, Wuppenal, West Germany) showed a time lag of approximately 6 seconds. The effect of such a time lag was considered insignificant in the calculation of the water permeability of hamster ova in the present study. The reason for the insignificance of the time lag is explained in Chapter 4 of this thesis.

The chamber design with top and bottom glass covers allowed a real-time recording of the cell volumetric behavior using a microscope-mounted video camera. The entire chamber fits on a typical microscope stage as shown in Figure 6.

A circular plastic spacer [~150 μm thick], with a hole in the middle [~1/8" I.D.] was inserted in the upper compartment. The thickness of the spacer protected the hamster ova [75-80 μm diameter] from being crushed between the dialysis membrane and the top cover glass. The spacer also decreased the volume of the upper compartment. This volume reduction increased the probability of finding a good ovum, since few ova were available for experimentation.
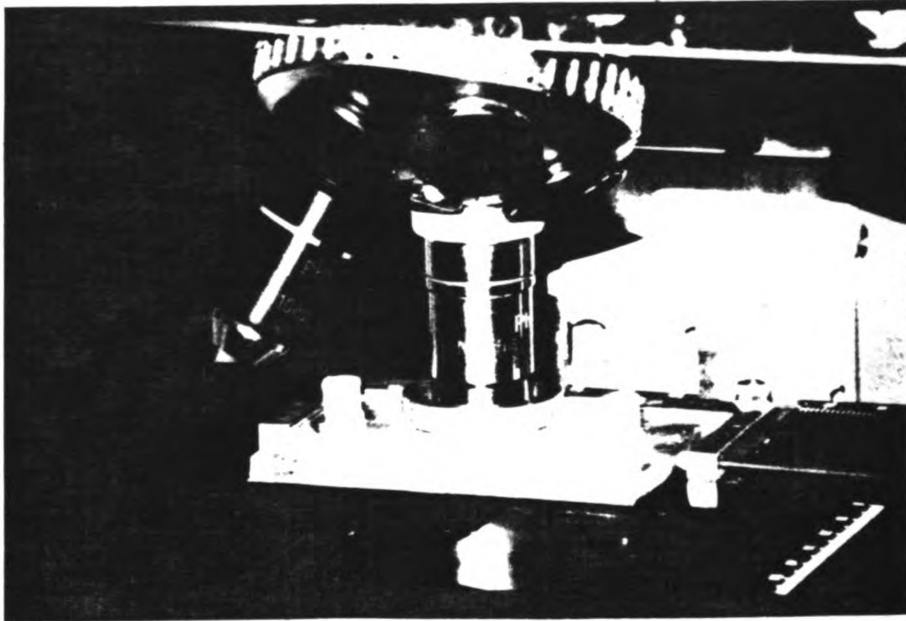
Figure 6. A photograph of the diffusion chamber
mounted on the microscope stage.

3.3 Measurement of "Osmotically Inactive Volume"

The concept of osmotically inactive volume was first proposed by Luké and McCutcheon (37). They modified the Boyle Van't Hoff law (see Appendix A) to account for the amount of solids and water inside the cell that is unavailable for transport across the cell membrane in response to an osmotic gradient. This amount of water and solids is usually defined as the "osmotically inactive volume".

The diffusion chamber described above was used in the present work to determine the osmotically inactive volume of unfertilized hamster ova. A small drop (~3 μL) of cell suspension containing 5 to 10 ova was placed inside the upper compartment. The upper compartment consists of 3 parts: 1) an upper bound, which is a cover glass; 2) a lower bound (an appropriate piece of dialysis membrane which was immersed for several minutes, before an experimental run, in a solution isotonic to the cell suspension [300 mOsm NaCl]) and; 3) the circular spacer described above, surrounding the sample region.

Next, the lower compartment of the chamber was mounted on the microscope and filled with isotonic NaCl solution [300 mOsm]. The assembled upper fixture was then press-fitted on top of the lower compartment (see Figure 5b). All experiments were conducted at room temperature [~23°C].

A healthy ovum was located in the microscopic field of view. The initial isotonic cell volume was recorded. The spherical nature of the hamster ova facilitated volume measurements from the circular projected area. Two or three diameters of the same ovum were measured. The mean of these diameters was used to calculate the volume of the spherical ovum.

The lower compartment was then flushed with a hypertonic sodium chloride solution. The ovum was observed to shrink until a new state of chemical equilibrium was established across the cell membrane. This was judged by observing no further change in the cell volume. At this point the new volume was recorded as mentioned above. The preceding procedures were repeated for the same ovum in a number of increasingly concentrated NaCl solutions. The new equilibrium volume was recorded each time. Figure 7 shows a sequence of photographs of typical microscopic observations of the equilibrium volumes of a single cell in increasingly concentrated NaCl solutions.

Figure 8 shows the typical behavior of a single ovum during osmotic shrinkage in hypertonic solutions. The linear relation between the inverse of the external solute concentration and the normalized equilibrium cell volume indicates the applicability of the so-called Boyle-Van't Hoff law (see Appendix A).
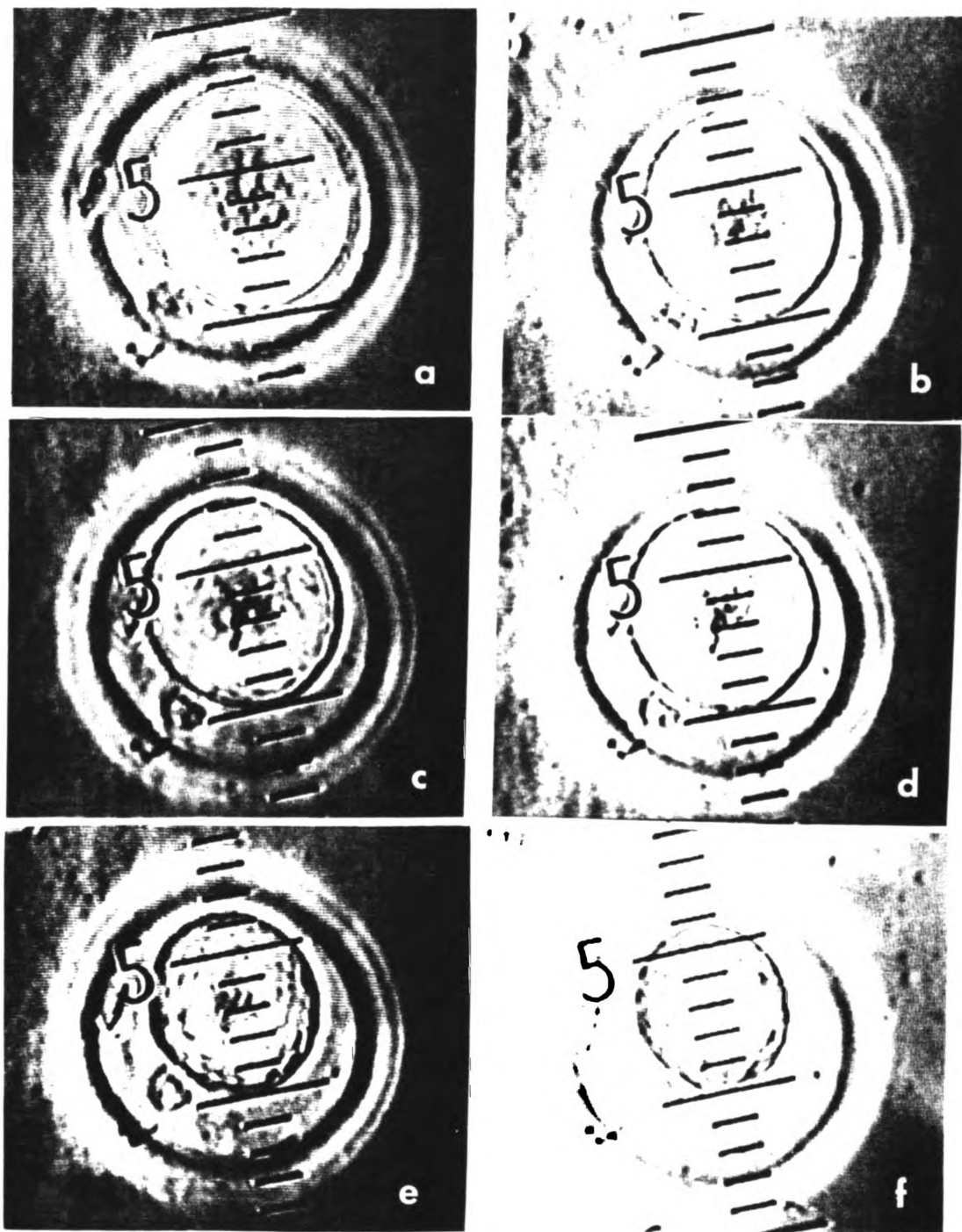
Figure 7. Sequence of photographs of equilibrium cell
volume in increasingly concentrated NaCl
solutions.(a-0.3, b-0.4, c-0.5, d-0.6,
e-0.8 and f-1.5 Osm)
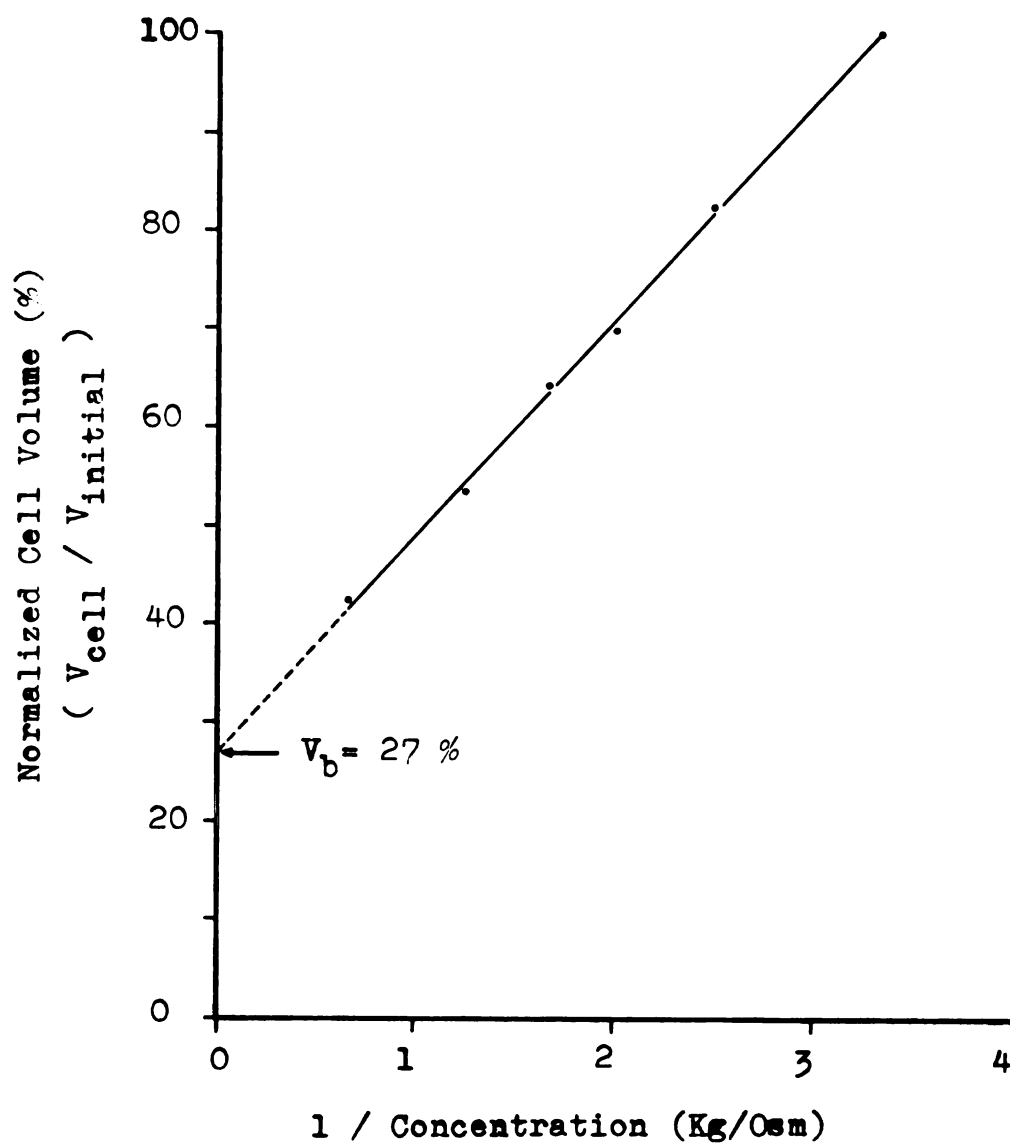
Figure 8. Typical equilibrium volumes
of a single ovum when
exposed to hypertonic
solute concentrations.

In order to generate a Boyle-Van't Hoff plot, the experiment as described above was repeated for several ova. The osmotically inactive volume of unfertilized hamster ova, was obtained by extrapolating the linear dependence to infinite solute concentration.

3.4   Measurement of Cell Membrane Water Permeability

The same diffusion chamber described above was used to determine the water permeability of hamster ova. The cell sample was placed in the chamber as explained in detail in the previous section. The initial volume was recorded. The bulk flow region was flushed with a hypertonic NaCl solution, using the flushing system described above. The moment at which flushing occurred was defined as time zero.

The actual transient cell response to the hypertonic salt solution was recorded on video tape. The tape was replayed and the cell volume was measured every 5-10 seconds, until the cell reached a final equilibrium volume in the concentrated salt solution. Substituting these measured volumes into Equation (2-18c), the normalized cell volume $\bar{V}$ was obtained. Then using Equations (2-18a) and (2-18b) the membrane hydraulic conductivity L_p was calculated.

3.5   The Cryomicroscope System

A temperature-controlled cryomicroscope conduction stage was used to observe the behavior of both protected

and unprotected hamster ova during the freezing process. The system is based on the designs of Diller and Cravalho (12) and McGrath et al. (14). It is essentially the same system used by Morris and McGrath (38) and Callow (26) with slight modifications (Appendix B).

As shown by Figure 9 the system consists of a specially designed heat conduction stage mounted on a commercial research light microscope (Zeiss Universal) to which a color video camera or a 35 mm camera can be attached. The video camera is connected to a video cassette recorder as well as to a color monitor. This allows the real-time observation of the sample behavior while simultaneously recording the same response on video tape. A refrigeration source, namely a liquid nitrogen (~196°C) dewar is connected to the conduction stage. A stream of two-phase nitrogen (vapor and liquid) is circulated in an annular cavity inside the copper stage (see Figure 10). A thermocouple and an electrical heater which exist on top of the copper block are both wired to an analog controller.

As shown in Figure 11, the controller mainly consists of an amplifier, a power supply, and a digital temperature display. The controller input is a programmed analog signal provided by a PDP-11 minicomputer through a digital-analog converter. A strip chart recorder is used to record the actual sample temperature profile.

The stage and the microscope optical elements are enclosed in an environmental glove box to minimize

41
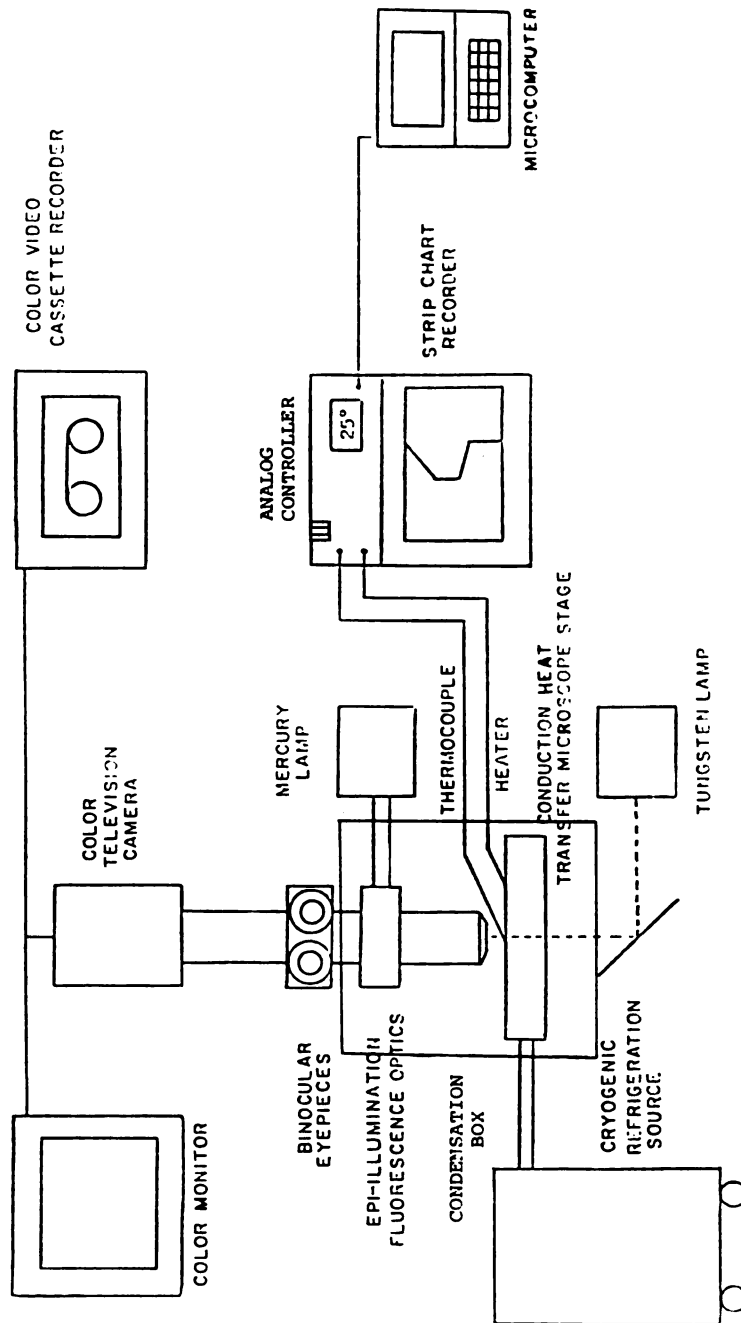
Figure 9. Layout of the cryomicroscope system.

NOT TO SCALE
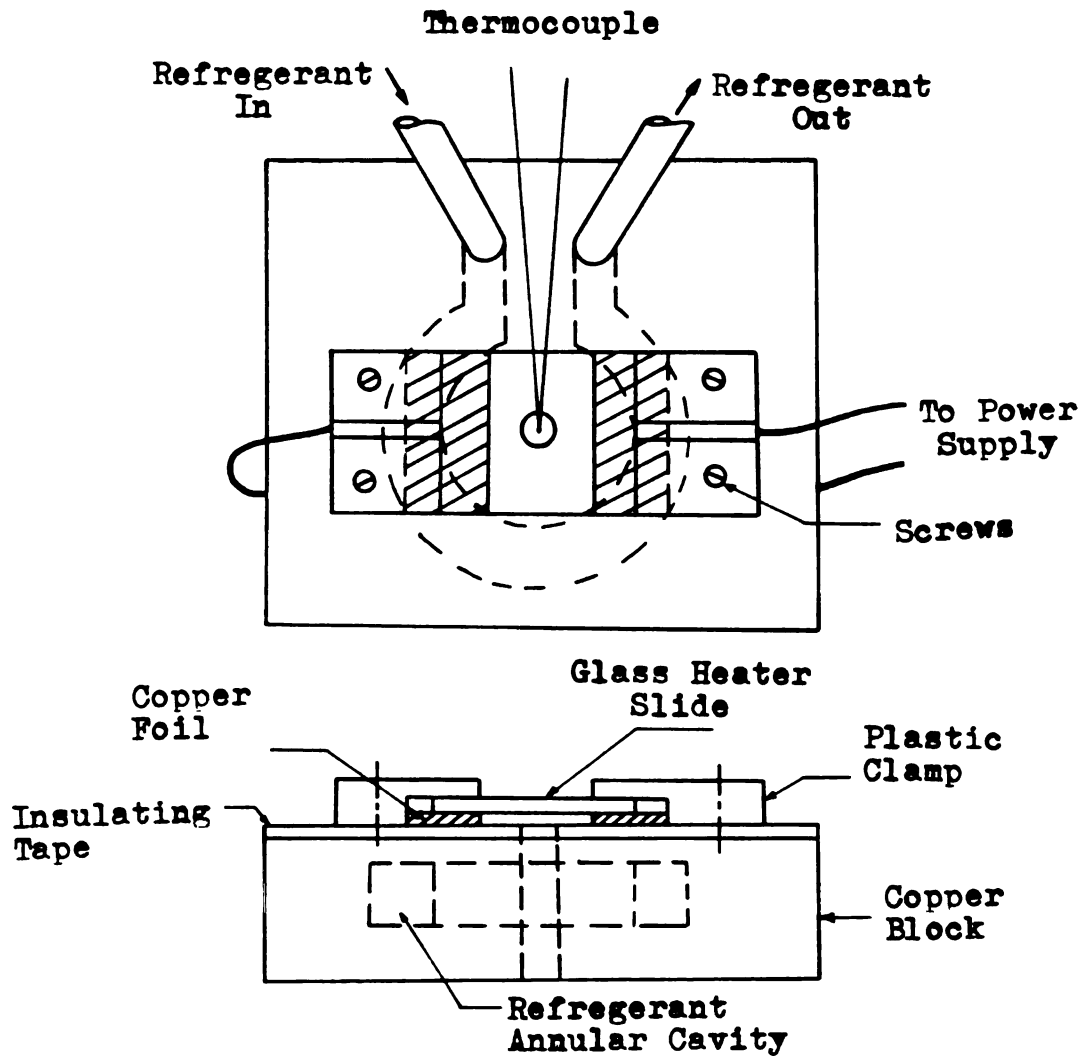
Figure 10. Schematic of cryomicroscope
conduction stage.
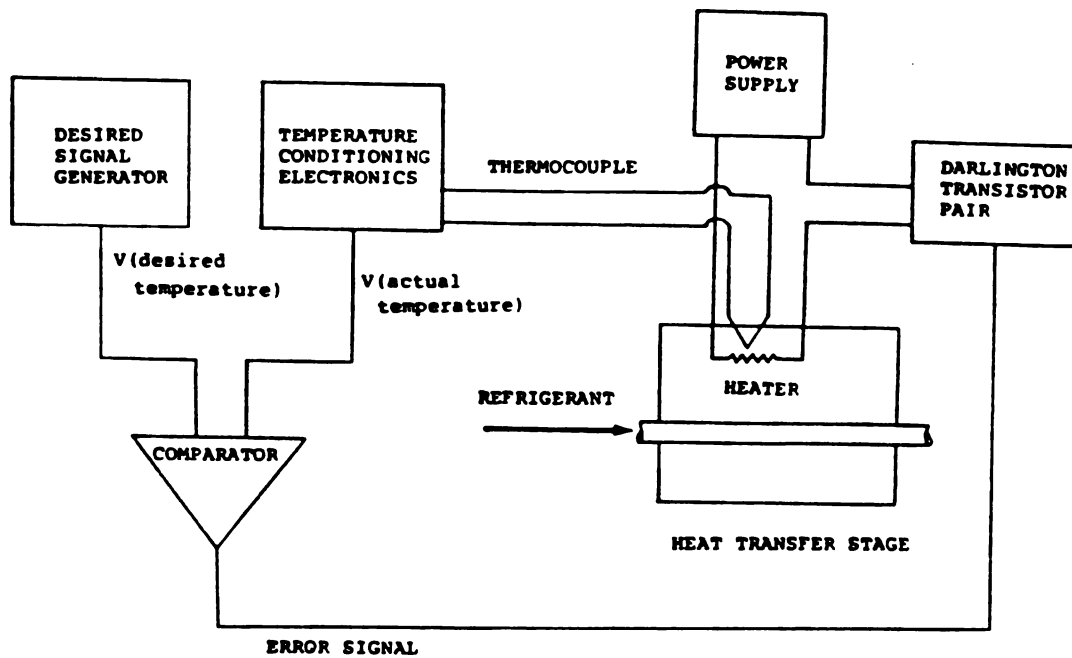
Figure 11. Schematic of cryomicroscope temperature controller.

condensation on the cryostage during freezing. The
assembly of the conduction stage is shown in Figure 10.
The body of the stage is a copper block that fits in
place of the regular microscope stage (Fig. 12). Interior
to the block is a circular channel of rectangular cross
section with inlet and outlet ports. The channel acts
as a passage for the refrigerant. A small hole is drilled
in the middle of the copper block to allow the transmission
of light through the metal base. The top surface of the
stage is covered with a thin layer of insulating tape.
A tiny copper-constantan thermocouple (copper wire no.
TFCP-003, Constantan wire no. TFCC-003, Omega Engineering
Inc., Stamford, CT) is sandwiched in between a regular
no. cover glass and the non-conductive surface of an
electrically conductive coated glass slide (1" × 1½" × 0.02",
E-C coated glass, no. 7059 Alkali Free, Corning, NY). An
epoxy glue (5 minute epoxy, Devcon Corporation, Danvers,
MA) or G.E. clear silicon rubber glue is used to hold
the thermocouple between the two surfaces. The entire
assembly is shown in Figure 13. The thermocouple-glass
sandwich is placed on the stage with the electrically-
conductive surface facing down, towards the insulating
tape. Two small pieces of thin copper foil contact
the edges of the lower surface of the sandwich to
facilitate supplying power across the thin film on the
bottom surface of the glass heater. The glass slide
is held on top of the stage by means of plastic clamps
at either end (see Figure 10).
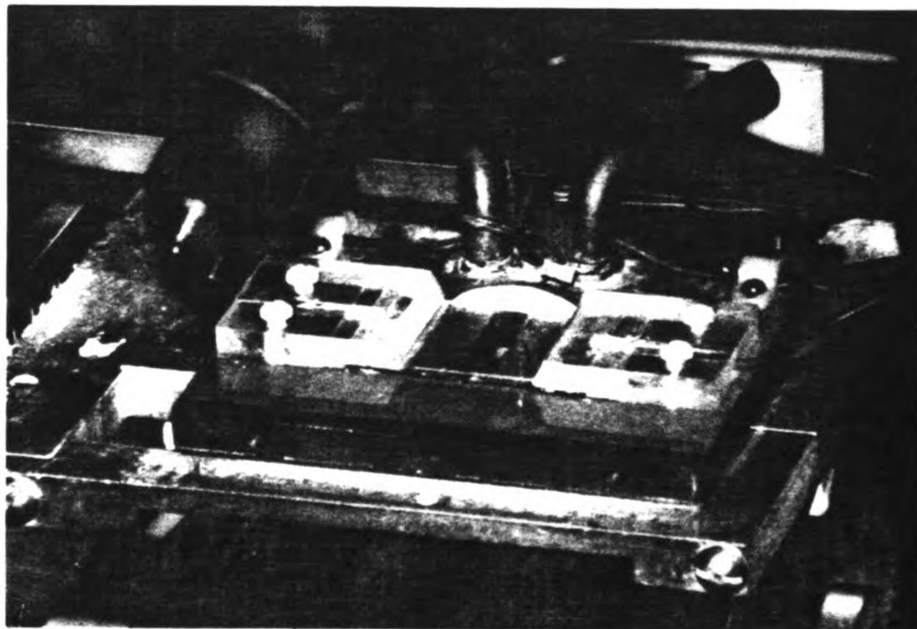
Figure 12. Photograph of cryostage mounted on the microscope.
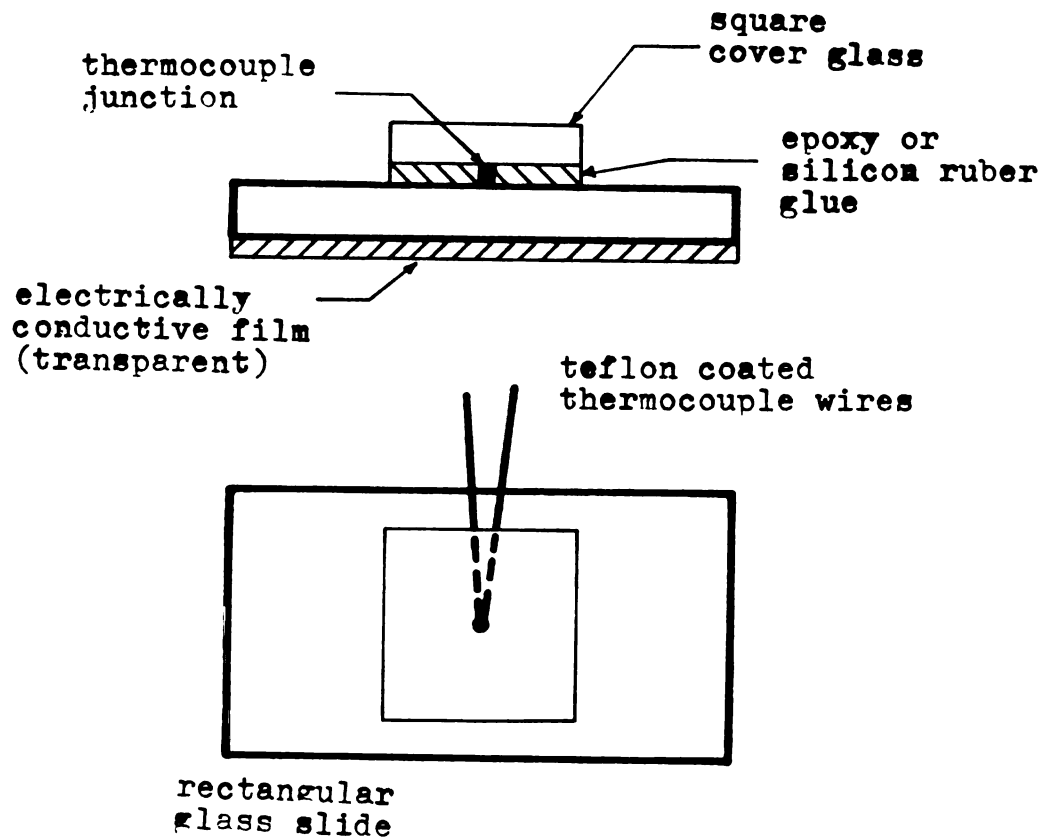
Figure 13. Assembly of the thermocouple
sandwich.

The manner in which the sample temperature is controlled is as follows. The sample is placed on top of the cover glass at the center of the viewing area as close as possible to the junction of the thermocouple. Saturated nitrogen vapor at approximately $-196°$ C is passed through the conduction stage, which acts as a thermal sink for the conduction of heat from the sample. A PDP-11 minicomputer provides an analog signal equal to the voltage equivalent of the desired temperature to the comparator of the control circuit. Simultaneously, the voltage equivalent to the actual temperature measured by the thermocouple is linearized, amplified and is input to the comparator. Measuring the difference between the desired and the actual voltages, the comparator induces the power supply to generate an amount of electrical power across the glass heater disk, which tends to drive the instantaneous temperature difference to zero. The digital temperature meter displays the actual temperature, while the strip chart recorded. traces the temperature history of the sample.

3.5.1 Error Introduced in the Measurement of Sample Temperature

Two major sources of error in temperature measurements are introduced due to the configuration of the conduction stage. The sample is vertically displaced from the thermocouple by the thickness of the glue layer and the coverslip above the thermocouple itself. This introduces

an amount of error that is estimated by Tu (39) to be less
than 1.0°C. The second and the most important source of
error is the horizontal displacement of the sample from
the thermocouple. Due to the normal operating mode of
the conduction type of cryomicroscope, a horizontal
temperature gradient is expected (40). While the
thermocouple is measuring the temperature at the very
local domain surrounding its junction, the sample
could be located anywhere in the viewing area of the
conduction stage. Consequently, due to the non-uniformity
of the temperature profile across the viewing hole, an
error in temperature reading could result from the
difference in temperature between the thermocouple
location and the sample location. This type of error
was studied in detail by Tu (39), who used a numerical
heat transfer analysis to determine the temperature
gradients in the vicinity of the thermocouple. However,
Tu used a different stage configuration than the one
used in this work. Callow (26) described an experimental
method for the determination of the total magnitude of
temperature error (in x and y directions). Callow
estimated that error to be as large as 8-9°C between
the thermocouple and the edge of the viewing hole
(~2 mm) at steady state.

The method used in the present work to estimate
the amount of temperature error in the horizontal
direction can be described as follows:

As shown in Figure 14a, an electrically conductive coated glass slide is prepared as described above (see Figure 13), with two more copper-constantan thermocouples sandwiched between the cover glass and the nonconductive surface of the heater slide. The distance between the middle thermocouple and each of the two additional thermocouples is 1.5 mm. The entire assembly was mounted on the conduction stage. The middle thermocouple was connected to the analog controller, so that the temperature of the center point in the viewing area can be controlled. Each of the other two thermocouples was connected to a digital voltmeter (DVM). The end of the copper thermocouple wire was connected directly to the positive pole of the DVM. The end of the constantan wire was connected to the negative pole of the DVM by means of a copper cable. The connection between the constantan wire and the copper cable was immersed in an ice bath for a reference. The temperature of the center point was set at values in the temperature range of (0 to -100°C) through thermocouple number 1. The voltages equivalent to the steady state temperatures at thermocouples 2 and 3 were recorded. The voltages were transformed into temperatures using the tables in the Temperature Measurement Handbook [Omega Engineering, Inc., Stamford, CT]. The generated plot in Figure 14b was produced from the measured values over the temperature range of 0 C to -100 C.
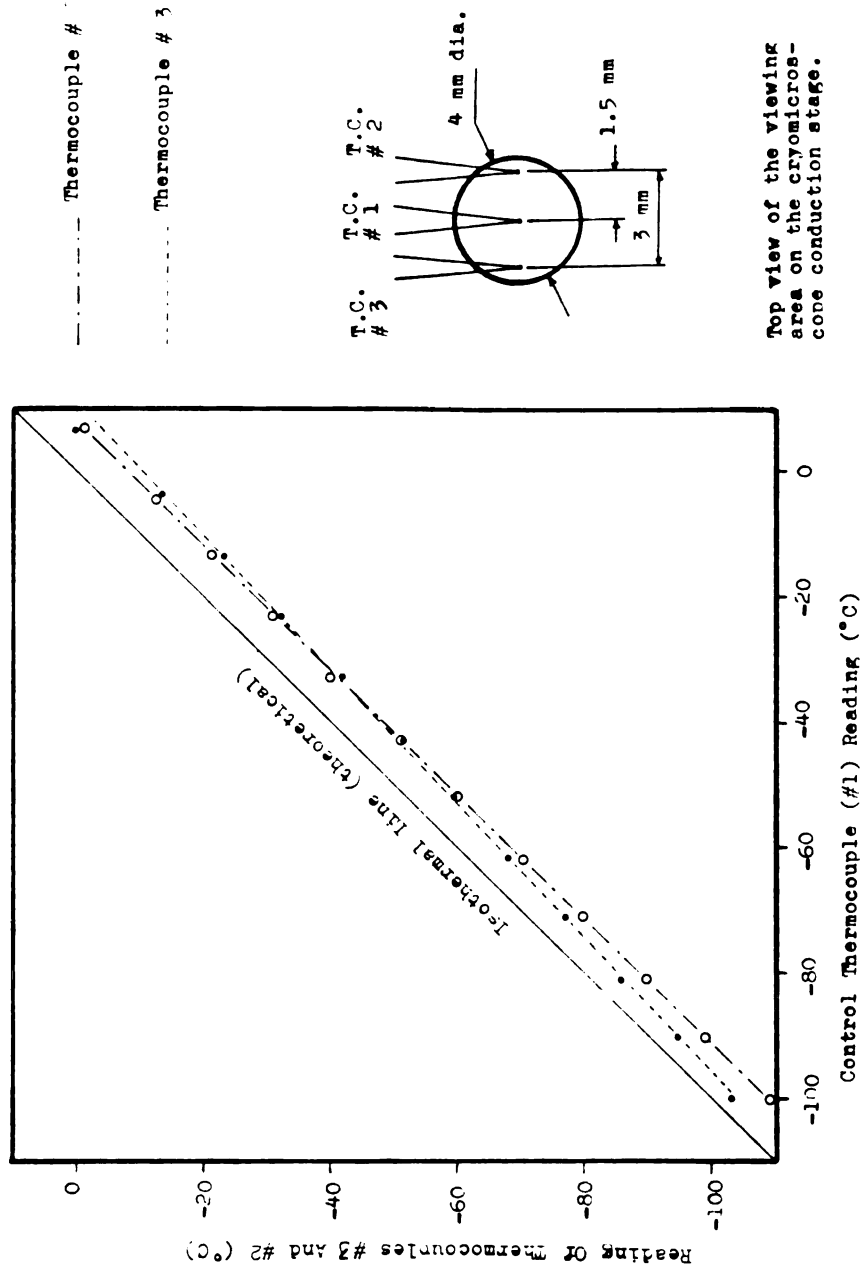
Figure 14. The estimated temperature error in the X-direction in the viewing area of the cryostage.

The steady state results shown in Fig. 14b give an amount of error ranging from 4°C to 10°C for a point displaced from the center of the viewing hole by 1.5 mm. This is in agreement with the results of Callow (26).

The fact that all data are below the theoretical line shown in Figure 14 indicates that thermocouple number one is always warmer than thermocouple number two and number three as expected.

The fact that thermocouple number two and number three data are not coincident on Figure 14 suggests that an undesirable asymmetry exists in the system. The most likely source of this asymmetry is the inaccurate positioning of the thermocouples relative to the center point of the viewing area and relative to each other.

To eliminate the horizontal type of temperature error as much as possible a cell very close to the thermocouple (no more than 0.3 mm away) was always chosen for observation. Hence, the overall steady state temperature uncertainty was estimated to range from 1.0°C to 3.0°C.

CHAPTER 4

RESULTS AND DISCUSSION

4.1   The Osmotically Inactive Cell Volume

Figure 15 is a Boyle-Van't Hoff plot, that shows the normalized cell volume $[V_{cell}/V_{initial}]$ as a function of the inverse of the solute concentration for ova. The data were gathered at room temperature [~23°C]. The data shown are the result of seven experimental runs. Each run was performed on a different ovum. The diffusion chamber was used as described in Chapter 3. During each run, a small drop of cell suspension was placed in the upper compartment of the diffusion chamber. A healthy ovum was located under the microscope objective, and its isotonic volume was recorded. The lower compartment of the chamber was filled initially with NaCl solution isotonic to the cell suspending medium [300 mOsm]. By changing the solution in the lower compartment, the single ovum was exposed to a number of increasingly hypertonic NaCl solutions [0.4, 0.5, 0.6, 0.8 and 1.5 Osm NaCl]. The ovum was allowed enough time to equilibrate in each hypertonic solution [~5 minutes]. The equilibrium cell
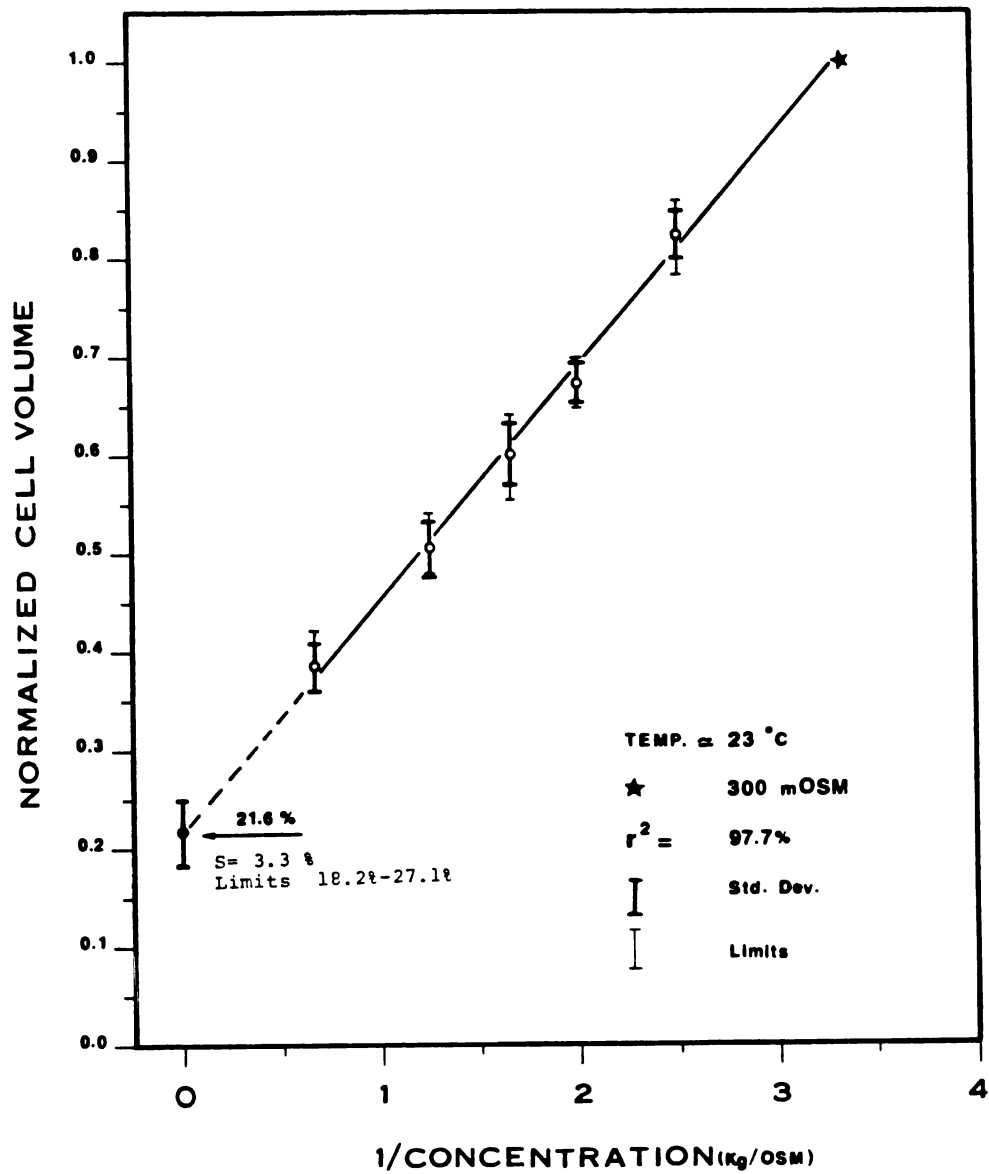
Figure 15. Boyle-van't Hoff plot

Each point is the mean of 7 ova suspended in NaCl solution. The data were fitted using the method of the least squares.

volume was recorded in each case and divided by the initial isotonic volume.

The ova seem to behave as perfect osometers, since the data show a highly linear relationship as expected from the Boyle-Van't Hoff law [see Appendix A]. The typical behavior of a single cell is shown in Figure 8, which also indicates a linear relationship for an individual ovum.

The line shown in Figure 15 is a least squares fit to the experimental data with a determination coefficient of 97.7%. The thinner "band" about each point represents the limits of the collected data, while the heavy marks represent the standard deviation with circles at the mean values. The fitted line is extrapolated to infinite concentration to yield an average osmotically inactive volume, V_b, of 21.6%, with a standard deviation of 3.3% and values ranging from 18.2% to 27.1%. At this time, there are no other values published for the osmotically inactive volume of hamster ova. But for a similar biological system, which possesses approximately the same volume (mouse ova) the published values are 18.2% [by Leibo (19)], and 20-21% [by Rall; see Leibo (19) for the values obtained by Rall]. This suggests that the present values are reasonable.
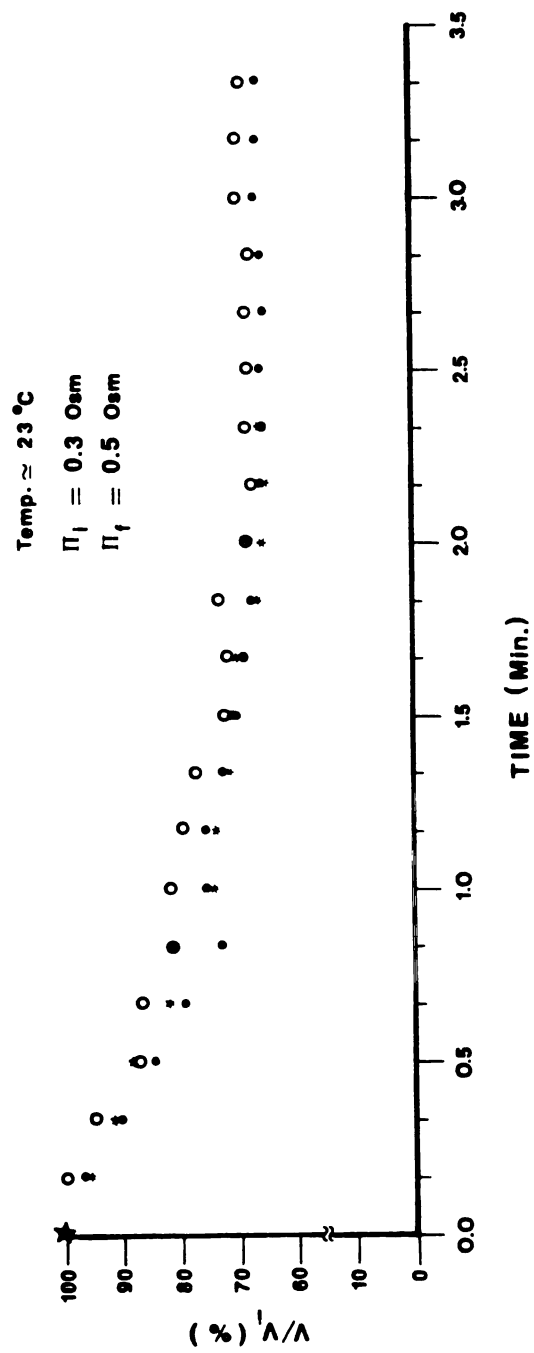
Figure 16. Representative shrinkage pattern of 3 hamster ova in a hypertonic NaCl solution as a function of time.

4.2   Cell Membrane Water Permeability

Figure 16 shows the normalized cell volume as a function of time for 3 hamster ova, when exposed to a hypertonic NaCl solution [500 mOsm NaCl].

The diffusion chamber described in Chapter 3 was used to generate the data in Figure 16. A small drop [~2 μL] of cell suspension was placed in the upper sample region. The lower bulk flow region was filled with a sodium chloride solution isotonic to the cell medium [300 mOsm]. A healthy ovum was located under the microscope objective. The initial cell volume was recorded as described above. The bulk solution region was then flushed with a hypertonic NaCl solution [500 mOsm], using the flushing mechanism described above. The moment at which the flushing occurred was marked as time equal to zero. The ovum responded to the hypertonic extracellular medium by shrinking. The transient cell response from time equal to zero until the cell reached equilibrium with the hypertonic external medium was recorded on a video tape. The equilibrium volume was judged by observing no further change in the cell volume. The video tape was replayed and the transient cell volume was measured from the projected area every 10 to 15 seconds. The transient volumes were normalized and plotted as shown in Figure 16. The same procedure was repeated for each one of 18 different unfertilized hamster ova examined in this

experiment. However, different final solute concentrations were examined ($\Pi_f = 0.5$, 0.8, 1.5 and 1.76 Osm). All experimental runs were conducted at room temperature ($T \cong 23°C$). Substituting the observed cell volume as a function of time into the equation developed by Terwilliger and Solomon (29) (Equation 2-18), Figure 17 was obtained. The solid line in Figure 17 is a least squares fit to the experimental data represented by circles. The slope of this line is equal to the water permeability L_p multiplied by the constant β, from which L_p was obtained for each single cell.

The x-intercept of Figure 17 represents the summation of two time lag factors. Due to the design of the flushing mechanism described above (see Chapter 3), the hypertonic solution will take some time to replace the isotonic solution first in the plastic tubing then in the bulk flow region. The second lag is the time constant associated with the solute diffusion across the dialysis membrane (this subject is discussed in detail in Chapter 3). The total time lag observed was typically 5 to 10 seconds. Fortunately, that lag did not affect the calculations of L_p, because as shown from Figure 17 L_p was calculated from the slope of the line, which should not change even if the line passes through the origin. However, it should be noticed that for perfect instantaneous mixing at time $t = 0$, the value of the y-variable of Figure 17 should be zero. The calculated
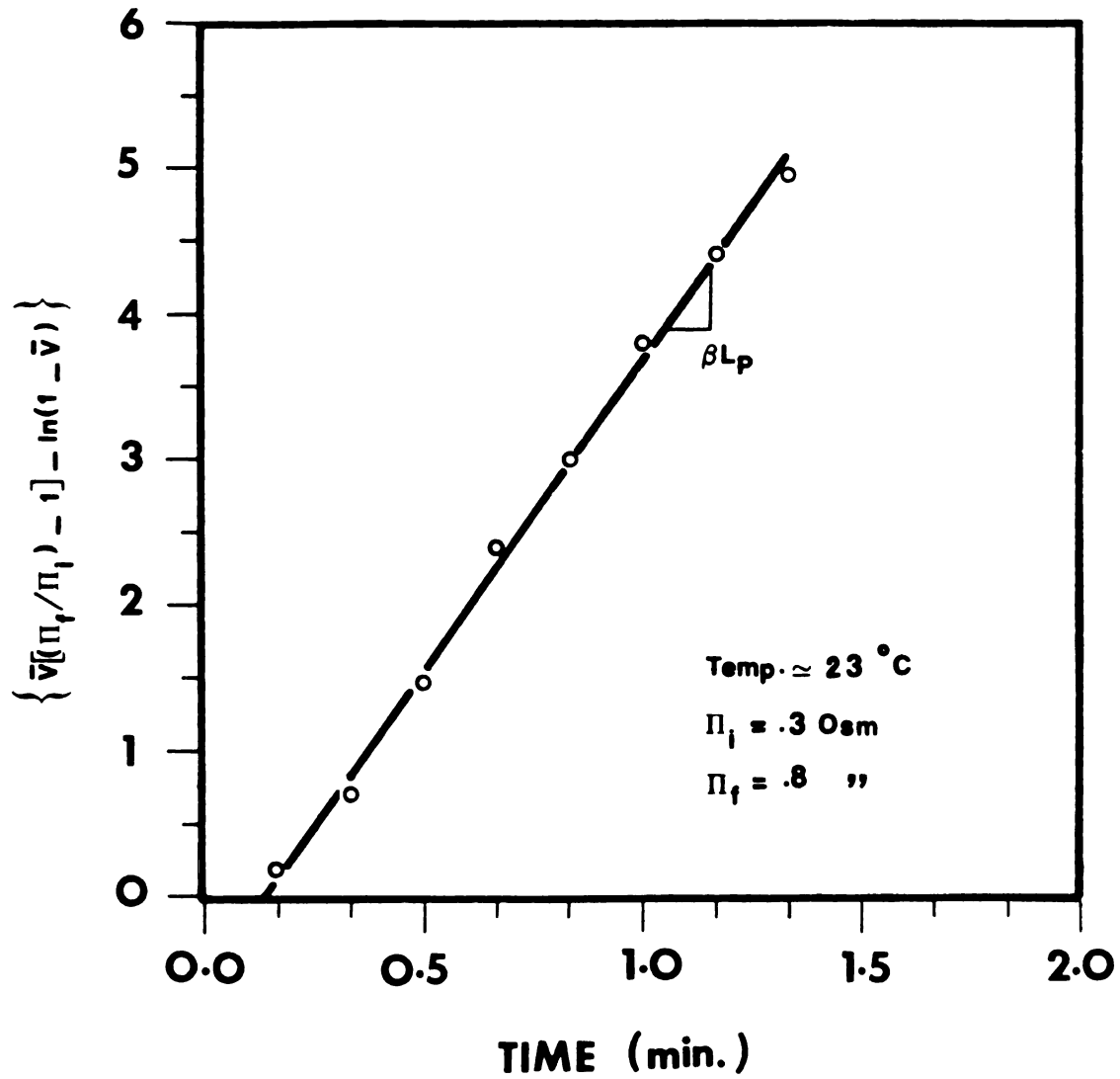
Figure 17. Representative correlation of experimental data in the form of Terwilliger and Solomon.

Calculated L_p = 0.815 $\mu m^3/\mu m^2 \cdot min \cdot atm$

$\widetilde{K}$ = 18.26 $\mu m/sec$

values of L_p were substituted back into the Terwilliger and Solomon equation, to produce the solid line shown in Figure 18. The line shows a good fit to the average experimental shrinkage pattern of 4 representative ova. This indicates that the dynamics of the osmotic shrinkage of hamster ova correlates to the mathematical model of Terwilliger and Solomon (29), and to the osmotic behavior of other biological cells, like human red blood cells which were examined by the same authors. L_p values ranging from $0.65 \rightarrow 1.00$ $\mu m^3/\mu m^2 \cdot min \cdot atm$ (corresponding to water conductivity $\tilde{\kappa}$ values from $16.3 \rightarrow 22.4$ $\mu m/sec$) were obtained with an overall mean value of 0.8 $\mu m^3/\mu m^2 \cdot min \cdot atm$ ($\tilde{\kappa} = 18.0$ $\mu m/sec$), at room temperature ($T \cong 23°C$).

The water permeability calculated above is approximately twice the published value for the permeability of unfertilized mouse ova (0.44 $\mu m^3/\mu m^2 \cdot min \cdot atm$ (19)). This indicates that unfertilized hamster ova are more permeable to water than mouse ova. Hence, during freezing, a hamster ova is expected to dehydrate faster than a mouse ova cooled to the same subzero temperature and at the same cooling rate.

Thus, according to Mazur's two-factor hypothesis (6), hamster ova have to be frozen at a faster cooling rate in order to observe the same probability of internal ice formation as that observed for mouse ova.

The effect of both temperature and solute osmolality on the water permeability of biological cells has been
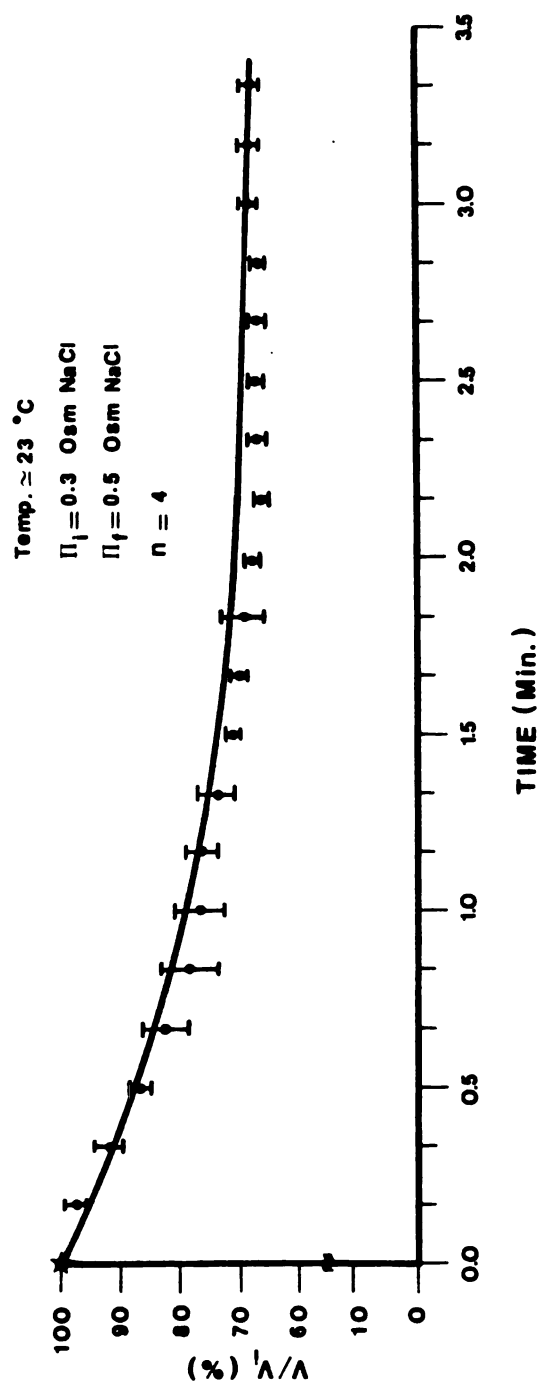
Figure 18. Normalized water loss from experiments compared to the mathematical model where $Lp = 0.7317 \frac{\mu m^3}{\mu m^2 \cdot min \cdot atm} (\equiv 16.39 \frac{\mu m}{sec})$. The curve fit shown uses the Terwilliger and Solomon form.

studied by a number of workers (19,30,41-47). There is

an agreement by most workers that the hydraulic permeability

L_p is highly dependent on temperature; this dependency

is usually presented in an exponential form as given by

Equation (2-19)

$$L_p = L_p\Big)_{T_g} \exp\left[-\frac{E_a}{R}\left(\frac{1}{T} - \frac{1}{T_g}\right)\right] \qquad (2-19)$$

The apparent activation energy, E_a, which describes the

temperature dependence of the hydraulic permeability

coefficient, L_p, for hamster ova was not determined in

the present study.

The computer simulation to be described later in

this thesis was performed using an activation energy

value of 14.5 kcal/mol. This value was obtained by Leibo

(19), for unfertilized mouse ova, and is the only

published value of activation energy for any ova. The

appropriateness of using this value for hamster ova will

be discussed later in this chapter.

Farmer and Macey (48), and Outhred and Colon (49)

reported that L_p is independent of the osmolality of

the suspending solution. Diller and Bradley (31)

suggested two forms for the solute concentration

dependence of L_p: exponential and linear as illustrated

by Equations (2-20) and (2-21),

$$L_p = L_p\Big)_{T_g} \exp\left[\frac{E_a}{R}\left(\frac{1}{T_g} - \frac{1}{T}\right) + E_c\left(\frac{1}{\Pi} - \frac{1}{\Pi_g}\right)\right] \qquad (2-20)$$

$$L_p = L_p\Big)_{T_g} \left[\exp\left[\frac{E_a}{R}\left(\frac{1}{T_g} - \frac{1}{T} \right) \right] + E_c\left(\frac{1}{\Pi} - \frac{1}{\Pi_g} \right) \right] \qquad (2\text{-}21)$$

Both equations when fitted to the experimental data obtained by the same authors (31) revealed poor statistical fits.

Scheiwe et al. (47) proposed another exponential form as shown by Equation (2-22),

$$L_p = L_p\Big)_{T_g} \exp\left[b\left(1 + a_2\, \frac{\Pi - \Pi_g}{\Pi_g} \right)\left(T - T_g \right) + a_1\left(\frac{1}{\Pi} - \frac{1}{\Pi_g} \right) \right] \qquad (2\text{-}22)$$

where a_1 and a_2 are functional parameters that can be adjusted to obtain the best possible fit to the experimental data. However, Scheiwe et al. (31) concluded that this method is rather approximate and that the values of a_1 and a_2 should be established independently in respective experiments.

Rich et al. (45) reported that the L_p of red blood cells decreases with increasing osmolality. Farmer and Macey (48) and Outhred and Colon (49) disagreed with the conclusions of Rich et al., where they reported that L_p is independent of the osmolality of the suspending medium. On the other hand Forster (50) fully supported the findings of Rich et al.

In this work, both the linear and exponential relationships between the hydraulic permeability of unfertilized hamster ova and the external solute concentration were investigated.

Figure 19 shows a linear fit to the data obtained for L_p at room temperature ($\sim$23°C) for different solute osmolalities [0.5, 0.8, 1.5 and 1.76 Osm NaCl]. The extracellular solute concentration is expressed in a form similar to Equation (2-21), $[1/\pi_i - 1/\pi]$. The light marks represent the range of L_p values at each solute concentration, while the heavy marks represent the standard deviation, with a circle at the mean value. The coefficient of determination is 66.3%. Figure 20 illustrates an exponential fit to the same data presented in Figure 19 with the same meaning of the drawn lines. The coefficient of determination for the exponential fit is 65%. Obviously, it can be noticed that the correlation coefficients of both the linear and the exponential fits are almost identical and that they are relatively low. This poor correlation can be attributed to the wide distribution of the measured values of L_p relative to the slope of the best fit line.

By means of a statistical test of hypothesis the slope of the best fit line in Figure 19 was found to be significantly different than zero at the 99% confidence level (see Appendix C). This means that the water permeability of hamster ova is dependent on the extracellular solute concentration in some fashion. However, it is not possible to assess the applicability of both suggested forms of dependence shown by Equations (2-20) and (2-21) due to the low correlation coefficients obtained above.
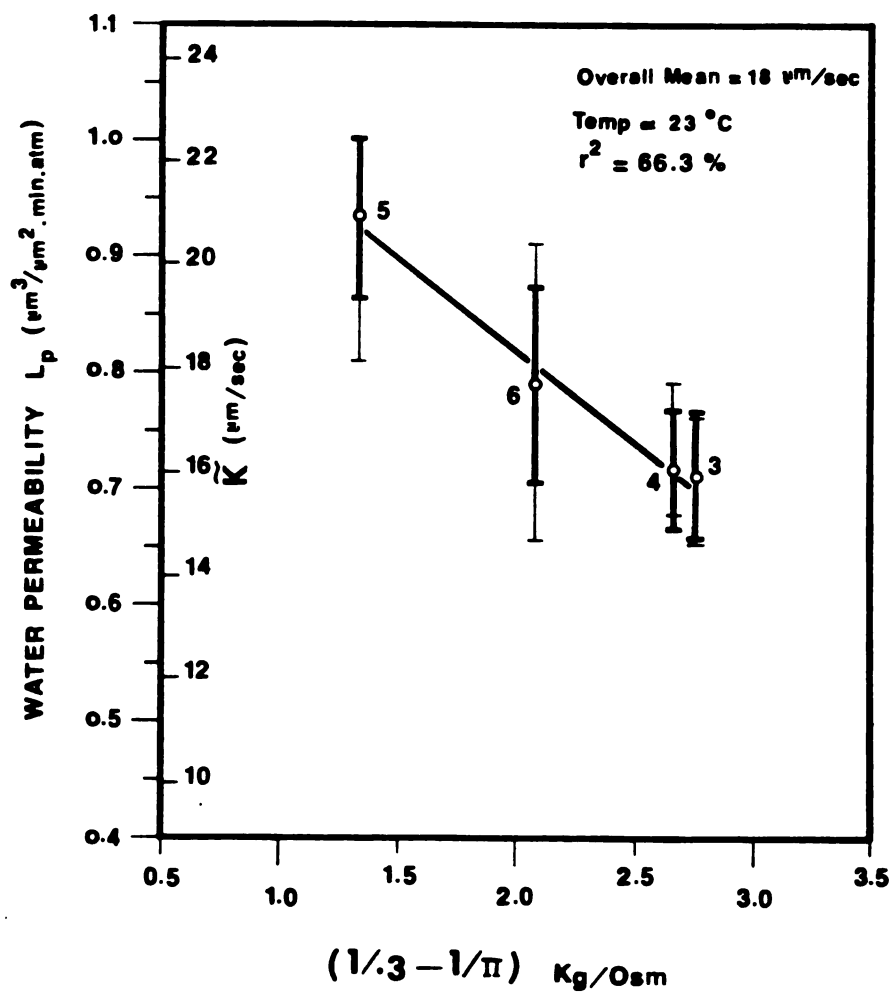
Figure 19. Water permeability as a function of the extracellular impermeable solute concentration (NaCl only).
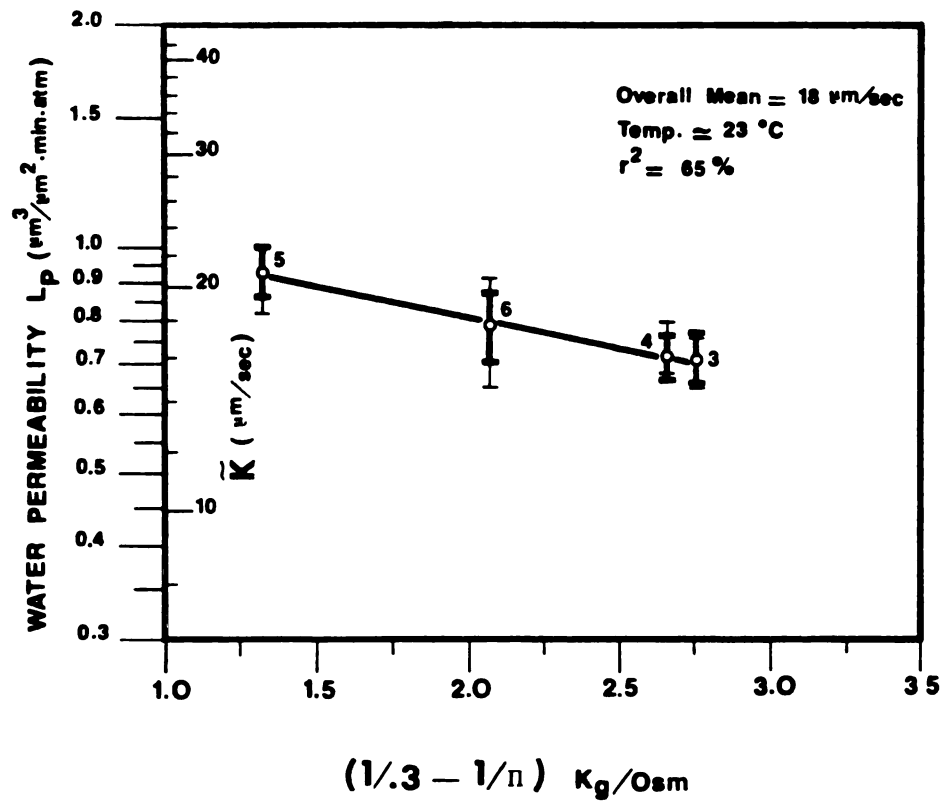
Figure 20. Water permeability as a function of the extracellular impermeable solute concentration (NaCl only).

The water permeability of hamster ova decreased by a factor of approximately 1.5 when the external solute osmolality increased from 0.5 to 1.76 Osm/kg. Since the solute osmolality increases to very high values during freezing, it was necessary to estimate the permeability values at such high solute concentration.

Extrapolating the statistical fit lines in Figures 19 and 20 to infinite solute concentration, where the value $(1/0.3 - 1/\Pi)$ is limited to 3.33 when $\Pi \to \infty$, the estimated values of L_p were found to be 0.607 and 0.627 $(\mu m^3/\mu m^2 \cdot min \cdot atm)$ for both linear and exponential relations respectively. These values are very close to the range of L_p values obtained in the present work (from 0.65 to 1.0 $\mu m^3/\mu m^2 \cdot min \cdot atm$). However, over the same range of solute concentration $[(1/0.3 - 1/\Pi)$ ranging from 0 to 3 kg/Osm], Schwartz and Diller (43) showed that the water permeability of granulocytes will decrease by at least an order of magnitude. Therefore, the external solute concentration dependence of L_p, for unfertilized hamster ova was considered insignificant. Hence, this concentration dependence of L_p was not accounted for in the computer model to be presented.

4.3   Computer Simulation of The Cell Osmotic Behavior During Freezing

4.3.1.   Assumptions

Several assumptions concerning the modeling of the osmotic behavior of biological cells during freezing are

regarded in this work. As reviewed by McGrath (8), one major problem involved in such models is the extrapolation of the numerical value of the membrane permeability at higher temperatures to lower subzero temperatures. Although some experimental evidence suggests that the extrapolation is valid, some researchers have suggested that it should be undertaken with care. Since physical and chemical events may alter the membrane transport characteristics at low subzero temperatures, the water permeability could undergo significant non-linear changes. However, in this work, the linear extrapolation was considered a reasonable assumption. An activation energy, E_a, of 14.5 kcal is chosen from the literature, as reported by Leibo (19) for unfertilized mouse ova. This value has been used unless otherwise noted. Some workers proposed that the concentration of the suspending medium affects the membrane permeability. However, from the experimental data presented above, the membrane hydraulic permeability is assumed to be independent of the solute concentration. It is also assumed that the solute concentration is uniform within the cell during freezing, which is generally accepted except for cells with very high water permeability (20,51,52).

Two cases may be considered for the cell membrane surface area during freezing: 1) it can be assumed to remain constant as assumed by Mazur (20) or; 2) it can be considered to behave like a shrinking sphere.

McGrath (53) mentioned that membrane material could be lost during freezing. However, Callow (26) showed that the difference in the predicted cell response during freezing, due to the surface area assumptions is not critical. Hence, the cell membrane surface area is assumed in the present work to be that of a shrinking sphere. This assumption is supported by Luke et al. (54). The membrane is assumed nonpermeable to solutes, hence, only water transport is accounted for in the dehydration model. A good approximation that is supported by analytical work (10,25,55), assumes that both the internal and external solutions behave like ideal solutions, and that the cell is in thermal equilibrium with its surrounding medium. Hence, no thermal gradient is assumed to exist within the cell boundary or in its local environment. Finally, it is assumed that the latent heat of fusion remains constant over the experimental range of temperature.

The computer model used in the present study is summarized at the end of Chapter 2 of this thesis. The initial solute concentration is taken to be that of the cell suspending medium [300 mOsm]. The inactive cell volume is taken to be 21.6%.

4.3.2   Effect of Cooling Rate on Predicted Cell Volume

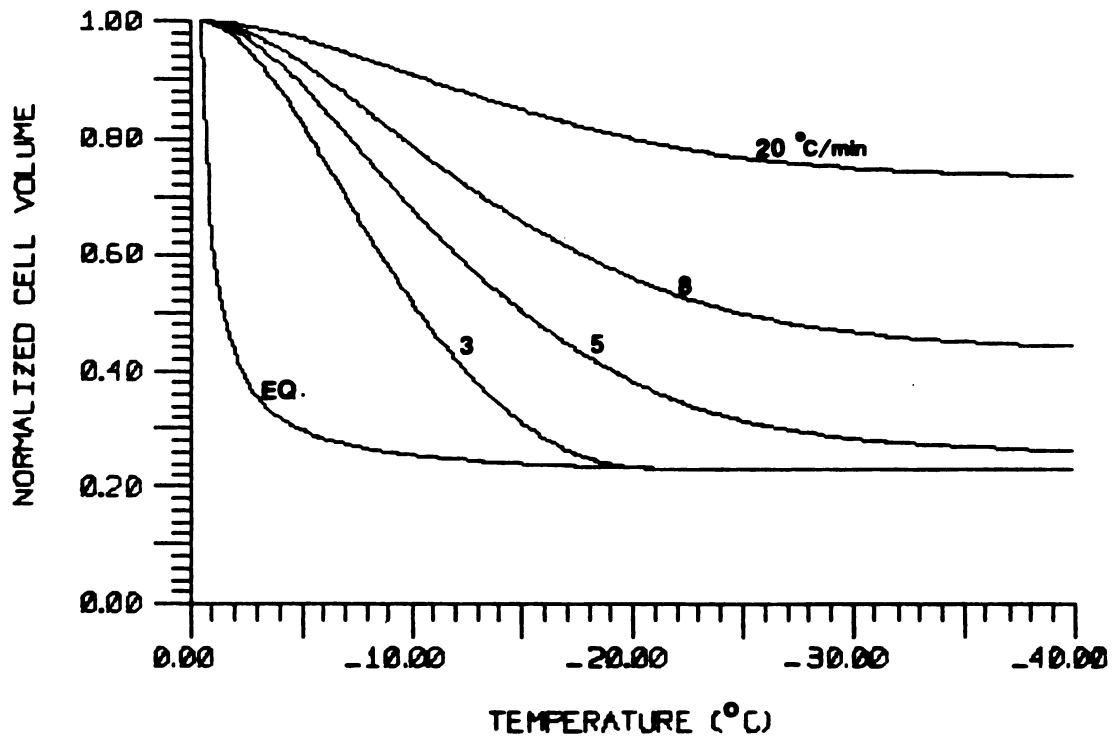Figure 21 shows the effect of changing the cooling rate, B (°C/min), on the predicted osmotic response of

Figure 21. Effect of cooling rate on predicted cell volume change during freezing [$L_p = 0.732 \dfrac{\mu m^3}{\mu m^2 \cdot min \cdot atm} \cong 16.4 \dfrac{\mu m}{sec}$]

unfertilized hamster ova. A typical L_p value of 0.732 $\mu m^3/\mu m^2 \cdot min \cdot atm$ obtained from the experiments performed as part of this work has been used, with an activation energy of 14.5 kcal/mol. The figure illustrates the highly significant effect of the cooling rate on the water content of an ovum at any intermediate subzero temperature. At ~-13°C the volume of a cell cooled at 3°C/min is about 45% of the volume of the same cell if cooled at 20°C/min. Consequently, at the same intermediate temperature the predicted volume of a cell cooled at a relatively faster rate is more displaced from the equilibrium volume. Hence, the cell is more likely to form ice internally. This correlates to the experimental results of increased probability of internal ice formation at higher cooling rates, as presented below.

4.3.3 Water Permeability Effect

Figure 22 shows the effect of the water permeability coefficient, L_p, on the predicted cell response during freezing. The solid lines represent the predicted response at cooling rates of 5 and 8°C/min using $L_p = 0.73$ $\mu m^3/\mu m^2 \cdot min \cdot atm$ ($\equiv 16.35$ $\mu m/sec$), while the dotted lines represent the response of the same cells using $L_p = 0.89$ $\mu m^3/\mu m^2 \cdot min \cdot atm$ ($\equiv 19.94$ $\mu m/sec$). Both L_p values are typical values obtained from the experiments performed for this thesis. Although these values are not the extreme limits observed for L_p (0.65 → 1.0 $\mu m^3/\mu m^2$
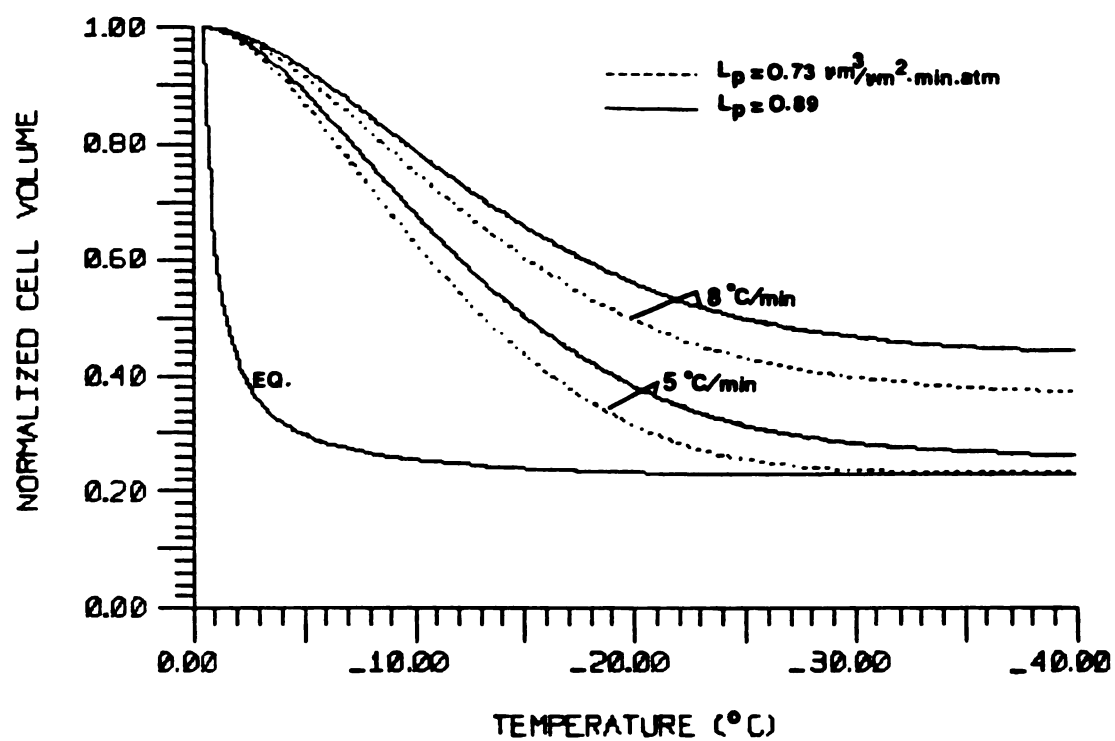
Figure 22. Effect of membrane hydraulic permeability (Lp) on predicted cell volume response during freezing. [1 $\mu m^3/\mu m^2 \cdot min \cdot atm \equiv 22.4$ $\mu m/sec$].

·min·atm), it can be noticed that these values represent

a major part of the total range of L_p values and these

values have a slight effect on the predicted cell response.

At an intermediate subzero temperature (-10 ~-15°C),

an increase of about 6% in the predicted volume is

associated with the indicated decrease in L_p, which

represents about 50% of the experimental range of L_p

values.

4.3.4   Activation Energy Affect

Figure 23 demonstrates the significance of the

activation energy, E_a, in predicting the cell osmotic

response during freezing. The solid line represents

the equilibrium cell volume as a function of subzero

temperature, and the predicted cell volume if it is

cooled at a rate of 8°C/min, using an activation energy

of 14.5 kcal/mol. This E_a value is reported in the

literature (19) for the unfertilized mouse ova system.

This value was chosen because of the lack of information

concerning the membrane transport characteristics of

the unfertilized hamster ova system, and because of the

biological and volumetric similarities between both

systems.

The dotted line represents the predicted response

of the same cell cooled at the same rate (8°C/min),

if the activation energy of the permeation process is

assumed to be 20 kcal/mol. This value was reported in
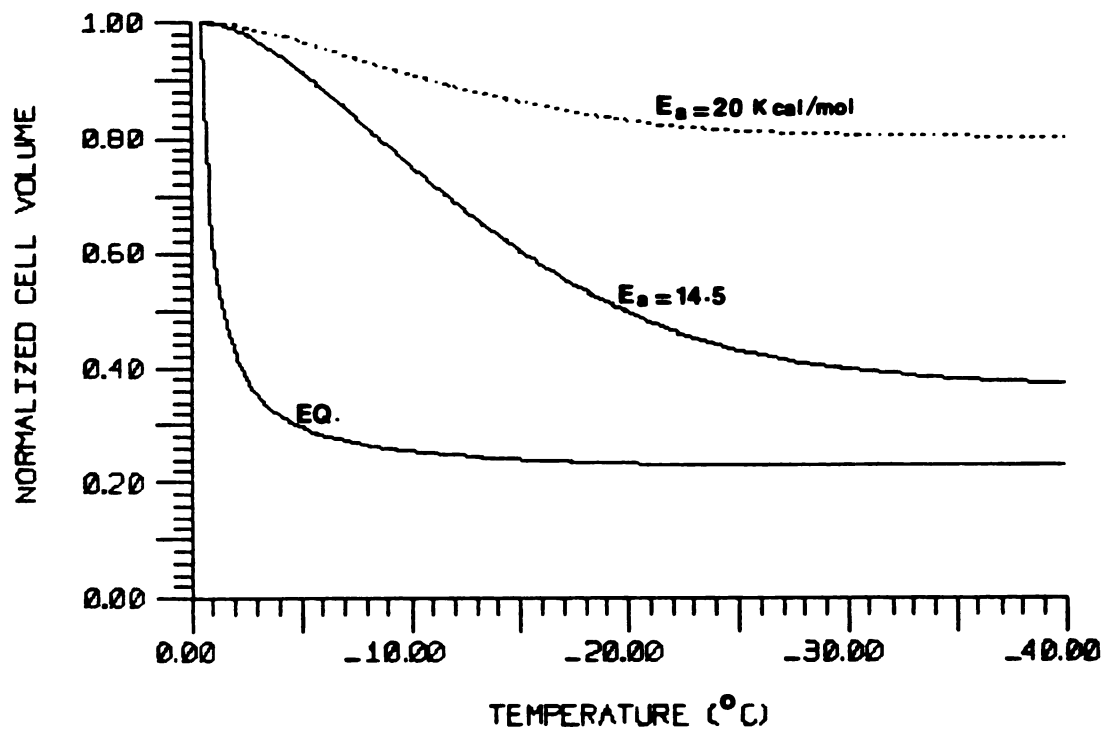
Figure 23. Effect of activation energy (Ea) on predicted cell volume response during freezing

[cooling rate (B) = 8 °C/min]

the literature (56) for Arbacia eggs, and is used here
only to demonstrate the effect of E_a on the cell response.
As can be seen from Figure 23, an increase of approximately
38% in the activation energy of the water permeability
can cause more than a 70% increase in the predicted cell
volume at -20°C, during freezing at a rate of 8°C/min.
This depicts the significant effect of the activation
energy on the predicted response as previously reported (20).
It also suggests that an accurate E_a value is required, in
order to minimize the sources of error in the modeling
process.

4.3.5 Comparison between Predicted and Observed Cell Volume Response During Freezing

Figure 24 shows the correlation between the predicted
cell response and the experimental data obtained by
freezing for 3 different hamster ova at a rate of 2°C/min.
Each set of data was obtained from the volume change of
one ovum in a separate run.

The normalized volume represents the cell volume at
defined temperatures divided by the initial cell volume.
The schematic in Figure 25 describes the problem associated
with the definition of the initial cell volume. In
Figure 25-a, the initial volume is defined as the volume
at 0°C. The entire set of volume measurements during
the freezing process will be shifted upward from the
computer prediction by approximately a 20-30% increase
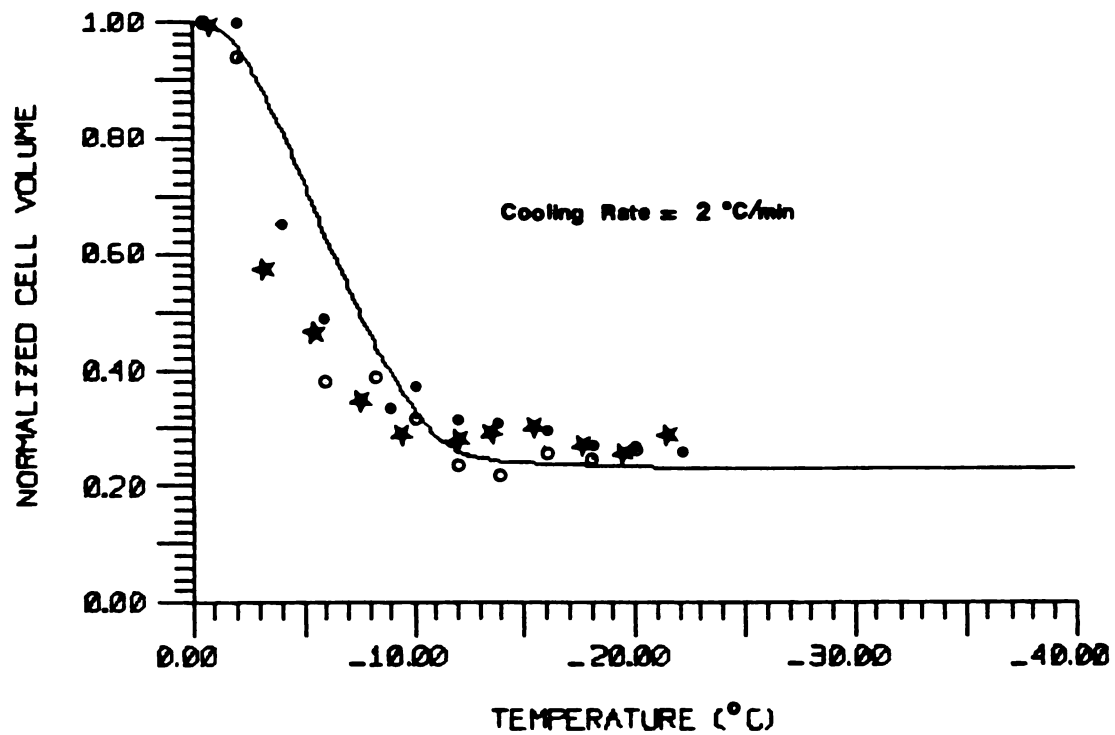
Figure 24. Comparison between predicted and observed cell volume response during freezing.

[cooling rate = 2°C/min]
V_b = 21.6°/.
Lp_{mean} = 0.8006 $\mu m^3/\mu m^2$·min·atm
$\bar{K}$ = 18 $\mu m/sec$
Average Dia. = 77 μm
E_a = 14.5 Kcal/mol
spherical shrinkage
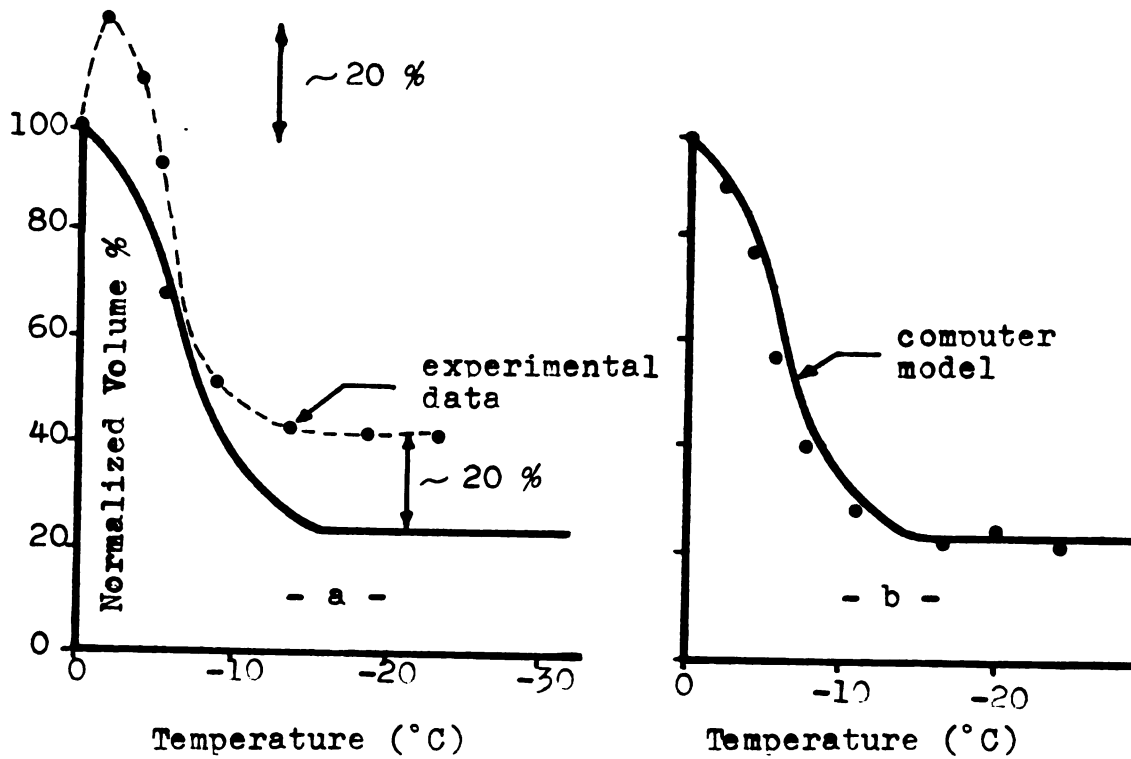
Figure 25. Schematic representing the fit of the
experimental data to the computer
model with initial volume defined as
a) 0.0 °C (before external ice appearance)
b) at the moment when external ice
surrounds the cell.

in volume. In Figure 25-b, the initial volume is defined

as the cell volume right at the moment when the external

ice completely surrounds the cell (~-1°C). The volume

measurements in this case will fit the computer model

in an appropriate manner. The reason for the volume

increase in the first case is believed to be due to a

deformation of the cell due to ice layers growing

underneath and/or above the cell. Hence, the second

definition of the initial volume is used here. In which

case the initial volume will not be the volume of a

sphere. However, it is assumed to be a sphere, having the

same diameter of the cell projected area.

Another source of uncertainty in the experimental

measurements is the distortion of the cell boundary by

the growing ice dendrites. Few ova stay spherical after

being surrounded by external ice. Therefore, due to the

small number of ova available for experiments, the number

of experimental runs presented in Figure 24 is not

adequate to justify the comparison between the model and

the actual cell response. Also, the overall steady state

temperature uncertainty is estimated to range from 1.0°C

to 3.0°C at the worst situation.

Other than the mechanical distortion of the cell

boundary by the external ice, the value of the activation

energy could be a second source of uncertainty.

The above discussion suggests that an accurate value

of the activation energy should be obtained. It also

suggests that data from a larger number of experimental
runs should be available, in order to justify any
conclusions on a solid statistical basis. In fact,
despite all uncertainties, the experimental data indicate
that the observed cell response is consistent with the
thermodynamic water transport model.

The observed cell response is also consistent with
the nucleation temperature measurements presented below.
At a cooling rate of 2°C/min, where no internal ice
formation was observed, the cells reached the equilibrium
volume at approximately -12°C to -14°C, while the mean
nucleation temperature is -13°C.

4.4   Nucleation Temperature as a Function of Cooling Rate

During freezing, the cell is initially in thermal
and chemical equilibrium with the surrounding aqueous
medium. As a result of heat removal from the medium,
ice starts to grow within the extracellular solution,
hence lowering the water chemical potential outside the
cell. The difference in chemical potential drives the
water flux out of the cell. The rate of water transport
across the membrane depends on the membrane water
permeability and the rate at which the system is cooled.
If the cooling rate is relatively fast, and the dehydration
rate is not rapid enough for the cell to achieve chemical
equilibrium, the cellular water freezes inside. This
event results in a decrease of the water chemical potential

inside the cell which re-establishes the chemical equilibrium across the membrane. The event of internal ice formation is commonly termed "nucleation", "flashing", or "blackening out" (13,57,58,60) because of the physical appearance. At sufficiently slow rates of cooling, the cell continues to dehydrate in order to maintain chemical equilibrium with the surrounding frozen solution. In such cases, "flashing" is not likely to occur. Nucleation temperature as a function of the cooling rate was experimentally determined for:

i) Unprotected Unfertilized Hamster Ova

Figure 26 shows the nucleation temperatures of unfertilized unprotected hamster ova as a function of cooling rate. The light bars represent the range of the data, the heavy bars represent the standard deviation and the circles represent the mean values with the number of cells indicated to the right of the mean. The nucleation temperature was statistically found to be independent of the cooling rate. At a level of significance of 0.01, the slope of regression line (not drawn) did not differ significantly from zero (Appendix C). The overall mean nucleation temperature for all cases was determined to be -13°C.

Despite cooling to a minimum temperature of -30°C, no internal ice formation was observed below the cooling rate of 4°C/min.
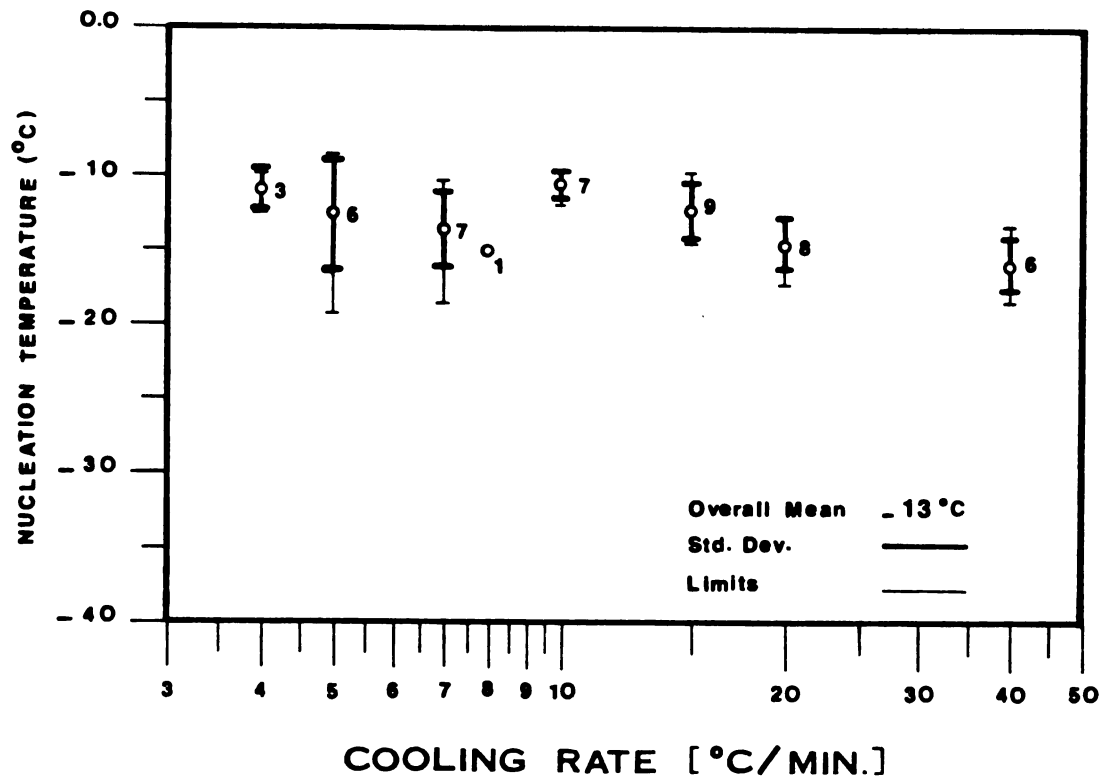
Figure 26. Nucleation temperature of unprotected unfertilized hamster ova as a function of cooling rate.

The probability of internal ice formation as a function of the cooling rate is illustrated in Figure 28. It shows 100% internal ice formation for cooling rates of 8°C/min and higher, and zero percent for cooling rates 3°C/min and lower. The dotted line was not fit statistically. It only serves to indicate an increase in the probability of internal ice formation with the increase in the cooling rate between the limits of 3 to 8°C/min.

Preliminary results of determining survival of unprotected unfertilized hamster ova as a function of cooling rate are shown in Figure 28. Morphological appearance was used to judge the cell survival after a freeze/thaw protocol. The figure illustrates a linear dependence between cell survival and cooling rate with a maximum survival of about 50% at a cooling rate of 3°C/min. For cooling rates of 10°C/min and lower, the thawing rate is 10°C/min. For cooling rates higher than 10°C/min, the thawing rate is the same as the cooling rate. The minimum freezing temperature reached was -30°C in all cases.

When Figures 27 and 28 are combined together (Figure 29), a number of conclusions can be drawn. At a cooling rate of 3°C/min, where no internal ice is observed, the cell "survival" (as judged by morphology), is maximum. Cell "survival" decreases with the increasing probability of internal ice formation until it reaches a
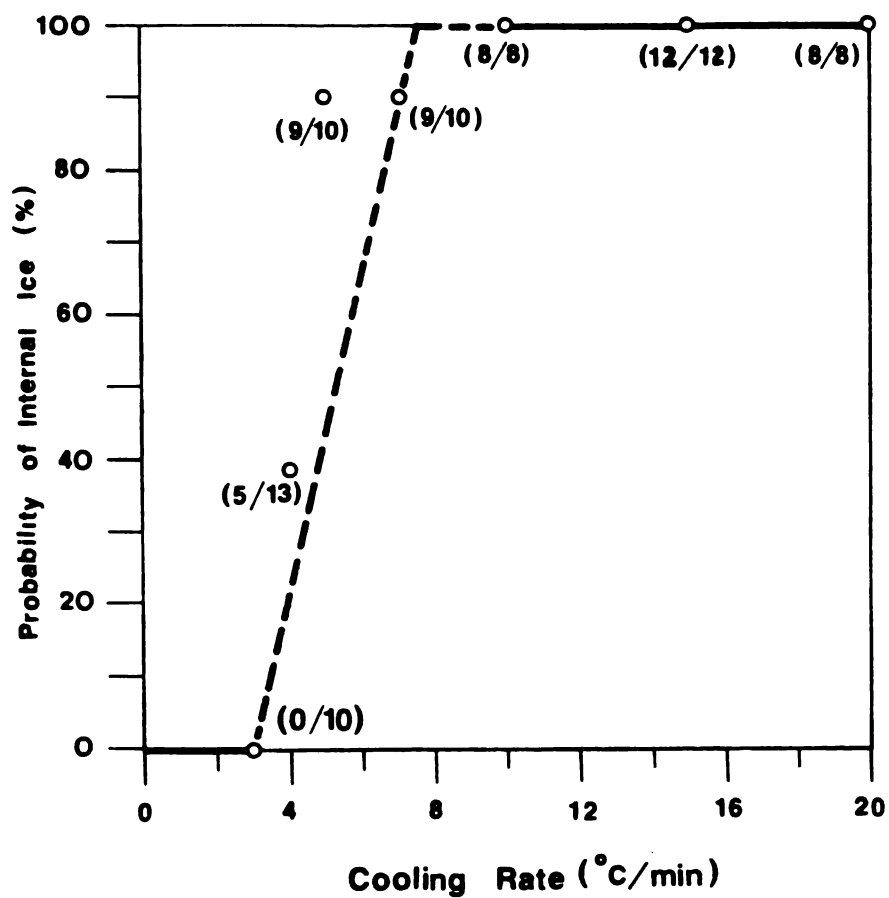
Figure 27. Probability of internal ice formation as a function of cooling rate for unprotected hampster ova.
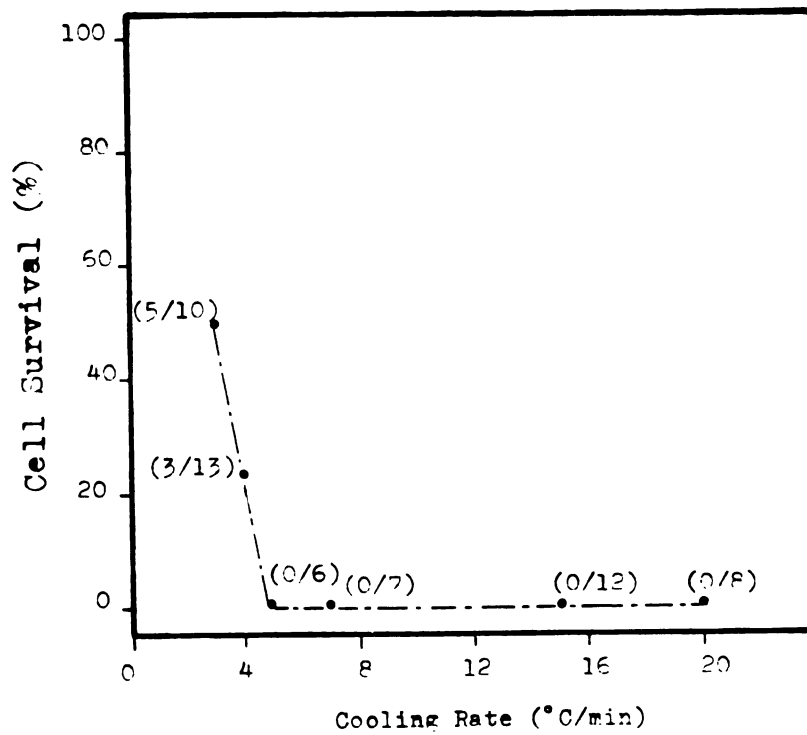
Figure 28. Unprotected hamster ova survival as
a function of cooling rate.
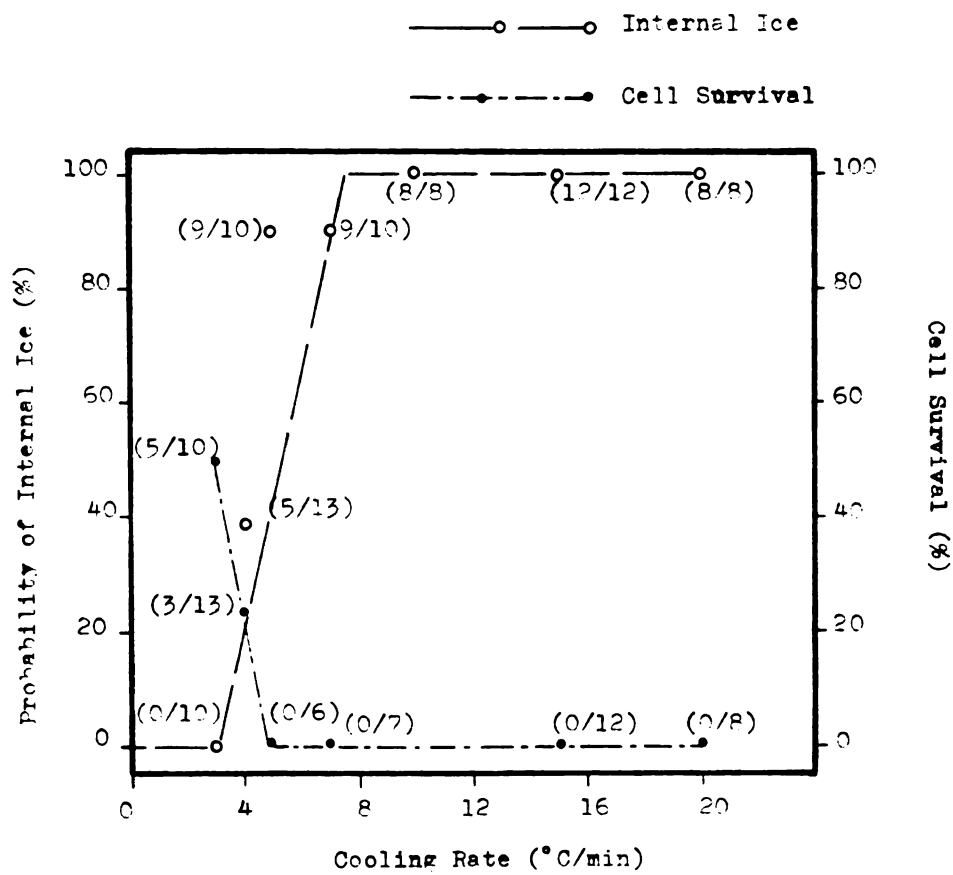
Figure 29. Probability of internal ice and cell survival both as a function of cooling rate.

minimum "survival". Hence, it can be concluded that cell survival is inversely related to the likelihood of intracellular ice formation. The same observation was reported for mouse ova suspended in 1 M DMSO (59).

ii) Protected Unfertilized Hamster Ova

Figure 30 shows the nucleation temperature as a function of cooling rate for unfertilized hamster ova suspended in 1.5 M DMSO. As can be seen, the collected data show large fluctuations and a wide range of nucleation temperatures. However, the overall mean temperature for all cells examined is shifted down to -57.1°C, which indicates that the cryoprotective additive (DMSO) has a significant effect on the nucleation temperature. Rall et al. (60) reported that permeating cryoprotective additives decrease the ice nucleation temperature of cells. The same authors also reported that intracellular nucleating agents become less effective in mouse embryos in the presence of glycerol or DMSO. They added that the nucleating agents become almost completely ineffective when the concentration of additive reaches 1.5-2.0 M. Rall et al. also reported that the nucleation temperature of eight-cell mouse embryos decreased from -10 to -15°C in saline alone to between -38° to -44°C in 1.0-2.0 M glycerol and DMSO.

The effect of cryoprotectives on hamster ova seems similar to the effect suggested by the mouse embryo
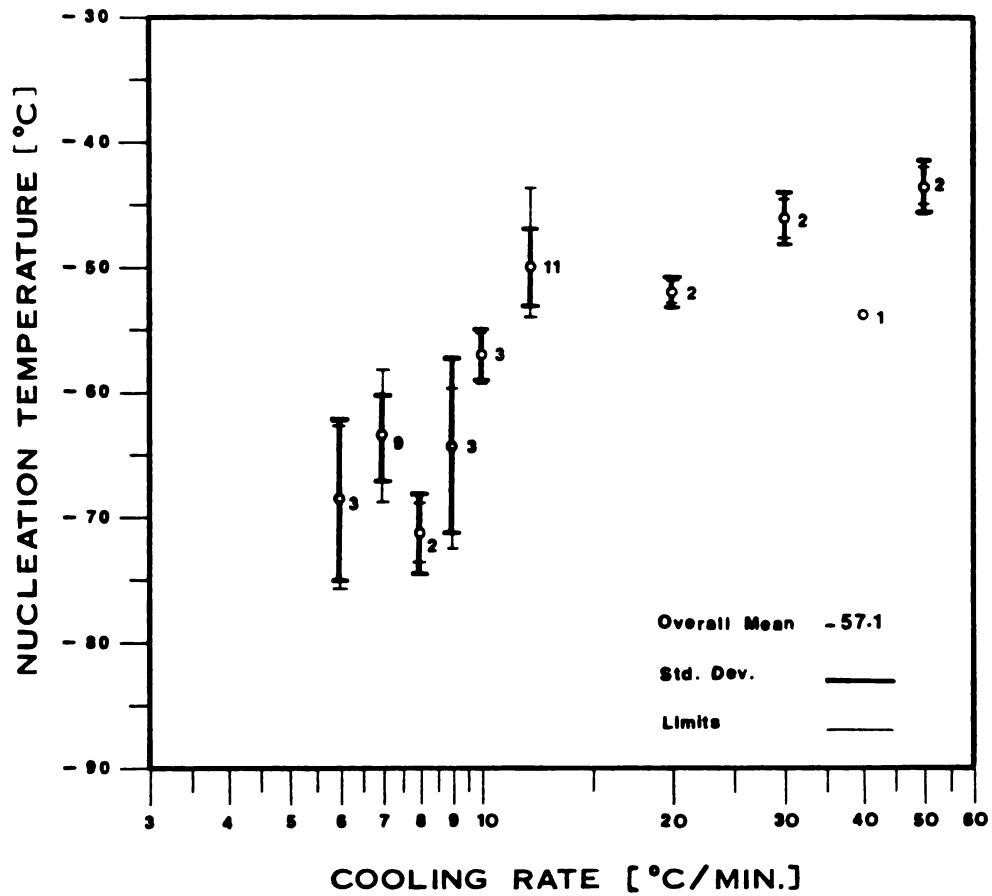
Figure 30. Nucleation temperature of protected
         unfertilized hamster ova in 1.5 M DMSO
         as a function of cooling rate.

results (60), where the overall mean nucleation temperature decreased from -13°C in saline to -57.1°C in 1.5 M DMSO solution.

The data in Figure 30 also suggest that the nucleation temperature at slower cooling rates is lower than that at fast cooling rates. This behavior was not observed for unprotected ova. It is also unlike that of unfertilized mouse ova frozen in 1 M DMSO cell suspension as reported by Leibo et al. (59). The minimum cooling rate below which no internal ice formation was observed was 6°C/min. This rate is approximately 6 times greater than that reported for mouse ova (1°C/min) (59). This correlates reasonably with the results obtained for water permeability, where the permeability coefficient for unfertilzied hamster ova is almost twice that reported for mouse ova (1).

CHAPTER 5

CONCLUSIONS

Based on the results of the experiments performed on the unfertilized hamster ova system in the present work, several conclusions could be made as presented below.

Unfertilized hamster ova behave as perfect osmometers. The Boyle van't Hoff law is applicable, and the mean osmotically inactive volume was found to be 21.6% with a standard deviation of 3.3%.

The value for the inactive volume agrees with the published values for mouse ova [18.2% (Leibo) and 20-21% (Rall)] which is approximately the same size as hamster ova [~75 μm dia.].

The dynamics of the osmotic shrinkage of hamster ova correlates to the mathematical model of Terwilliger and Solomon (29) and to the behavior of other biological cells.

The calculated water permeability of unfertilized hamster ova (0.8 $\mu m^3/\mu m^2 \cdot min \cdot atm$) is approximately twice the published value for mouse ova (0.43 $\mu m^3/\mu m^2 \cdot min \cdot atm$) obtained by Leibo (19). This suggests that a faster

freezing rate will be required in order to observe the same probability of internal ice formation during rapid freezing.

As predicted from the water permeability results, internal ice started to form at much higher cooling rates (4 and 6°C/min for unprotected and protected hamster ova respectively) than in the case of mouse ova (~1.0°C/min for protected ova).

The external solute concentration appears to affect the water permeability, since it decreases the permeability by a factor of approximately 1.5 when the external concentration increases from 0.5 to 1.76 osm/kg. The concentration dependence of the water permeability is less pronounced than for some other systems. A low coefficient of determination of (~66%) was obtained as a result of the wide range of the calculated water permeability values. This precludes concluding that the concentration dependence is significant with a high degree of confidence.

A thermodynamic computer model shows a slight effect of the range of L_p on the predicted cell response during freezing. It also shows the large effect of the activation energy E_a on the predicted response, which indicates that an accurate value of E_a should be obtained.

The observed cell volume response during freezing correlates well with the predicted response using a published value of the activation energy for the mouse

ova [14.5 kcal/mol (Leibo]. The comparison suggests that E_a for the hamster ova is quite similar but slightly less than that of the mouse ova.

At the 0.01 level of significance, the nucleation temperature of unprotected hamster ova was found to be independent of the cooling rate with an overall mean of -13°C.

For ova protected in 1.5 M DMSO the system showed large fluctuations in the nucleation temperature as a function of the cooling rate. However, the overall mean is shifted down to -57.1°C. The data suggest that the nucleation temperature at slower rates is lower than that at rapid rates. This response is unlike that of the mouse ova system as reported by Leibo et al. (11), because for the mouse ova system the experimental observations suggested that over the range of about 2-40°C/min, the nucleation temperature is relatively independent of cooling rate (59).

CHAPTER 6

SUGGESTIONS FOR FUTURE WORK

At this point, some suggestions are made for future work, on the modeling of the freezing response of hamster ova and, the design of optimal freeze/thaw protocols that yield maximum survival.

1) Determine the activation energy for the water permeability of the hamster ova membrane. A low temperature bath and a modified version of the diffusion chamber could be used in conjunction with the method presented here for room temperature experiments to determine membrane water permeability values at lower temperatures.

2) Develop an accurate method for measuring the cell volume during freezing. An image analysis technique could be used to measure the projected area of an ovum. However, for a more accurate volume measurement a three-dimensional image has to be constructed.

3) Collect more data regarding the cell response during freezing. Such data is required to judge the validity of the thermodynamic model as well as the assumptions included.

4) Characterize the thawing behavior of hamster ova and correlate that to a consistent thermodynamic model.

5) Minimize the amount of error introduced in the measurement of temperature due to the thermal gradients present within the viewing area of the microscope freezing stage. A modified design for the cryostage based on the analysis of Tu (39) and other workers could be helpful.

6) Collect more data regarding the survival of hamster ova and the formation of internal ice, both as a function of cooling rate. Such data could help define the mechanism of cell injury during freezing.

7) Use fluorescent markers (FDA) for viability assays, a technique that has been developed by McGrath et al. (14). Data is also available from DeMayo (34).

8) Determine the effect of different types and concentrations of cryoprotective agents on the nucleation temperature of hamster ova. Data is available from DeMayo (34).

9) Study the effect of *in-vivo* and *in-vitro* fertilization and development on both the membrane transport characteristics and the formation of internal ice.

APPENDICES

APPENDIX A

APPENDIX A

BOYLE VAN'T HOFF LAW AND THE
OSMOTICALLY INACTIVE VOLUME

The cell membrane is assumed to be semipermeable, which means that it allows for transmembrane water flux but not for solute transport. This assumption implies that in the case of osmotic equilibrium,

$$\mu_w^i = \mu_w^o \qquad\qquad\qquad (A-1)$$

This means that the chemical potential of water should be equal on both sides of the cell membrane for the equilibrium situation.

At this point a distinction should be made between two independent driving forces each of which can cause transmembrane water flux. These forces are, Δp, the hydrostatic pressure difference and, $\Delta \pi$, the osmotic pressure difference that results from the difference in solute concentration on both sides of the membrane. At equilibrium, $\Delta \pi$ is numerically equal to Δp, however $\Delta \pi$ is best thought of as a measure of water activity or concentration since

$$\pi = \frac{-RT \ln a_w}{\overline{V}_w} \qquad (A-2)$$

where, $\overline{V}_w$ is the partial molar volume of water.

As summarized by McGrath (8), the Boyle Van't Hoff law states that the osmotic pressure of a solution varies inversely with the volume of solvent in which a definite quantity of the solute is dissolved.

$$\pi V_w = \text{const} \qquad (A-3)$$

where, V_w represent the volume of water (solvent).

Hence, the total volume of the cell should vary inversely with the osmotic pressure of the extracellular solution. The Boyle Van't Hoff law is valid only if there is no hydrostatic pressure gradient across the cell membrane, if the temperature is constant, if the intracellular solution can be considered ideal, and if solute leakage across the membrane does not occur.

The Boyle Van't Hoff law is corrected for any osmotically inactive volume that may be present within the cell, hence,

$$\pi (V_{cell} - V_b) = \pi_i (V_i - V_b) \qquad (A-4)$$

where, V_{cell} is the total cell volume, V_b is the osmotically inactive volume, and the subscripted values π_i and V_i correspond to a reference intitial state.

Rearranging Equation (A-4) results in the final form of the Boyle Van'tHoff law:

$$\frac{V_{cell}}{V_i} = \frac{V_b}{V_i} + \frac{\pi_i}{\pi} \left(1 - \frac{V_b}{V_i}\right) \qquad \text{(A-5)}$$

where V_{cell}/V_i is the normalized cell volume, and V_b/V_i is the normalized osmotically inactive volume.

The so-called Boyle-Van't Hoff plot is determined experimentally by exposing the cell to solutions of increasing osmotic pressure, and recording the equilibrium cell volume in each concentrated solution. The resulting linear relationship between the normalized cell volume and the inverse solute concentration $(1/\pi)$ (if it exists) is extrapolated to infinite solute concentration $(1/\pi = 0)$ to estimate the normalized osmotically inactive cell volume.

APPENDIX B

APPENDIX B

DESIGN MODIFICATIONS OF CRYOMICROSCOPE
CONDUCTION STAGE

In previous designs of the crysostage two configurations were used to hold the electrically conductive heater slide on top of the copper block, while maintaining good contact with the poles of the heating circuit. The first configuration used a circular quartz disc of 0.075" thickness. The quartz disc was bonded to the insulating tape covering the copper block with a commericial silver based paint. This paint served as both an electrically conducting medium and an adhesive. However, in an attempt to increase thermal response times by decreasing thermal mass, Callow (26) used thinner quartz discs (0.025" thick). This resulted in frequent breaking of the quartz disc and/or the breaking of the silver paint-quartz disc bond. Callow solved this problem by painting the edges of the quartz disc onto a thin strip of aluminum foil, and the aluminum foil was painted down on the insulating tape. Although this arrangement solved the breakage problem, it decreased the thermal response time of the quartz disc since the disc is not in optimal contact with the thermal sink.

In the present study a rectangular glass slide
(1" × 1½" × 0.02") which is coated with a thin transparent
film of electrically conductive material on one surface,
was used instead of the circular quartz disc. The edges
of the glass slide were clamped to the copper block
by means of two plastic clamps screwed in the copper
base (see Figure 10). Two pieces of thin copper foil
were inserted between the conductive surface of the
glass slide and the insulating tape to connect the
conductive surface to the heating circuit. This
arrangement solved the breakage problem resulting from
the thermal stress present in the glass slide during
freezing. It also improved the thermal contact between
the glass slide and the heat sink (the copper block),
hence improving the thermal response time.

In the previous design of the thermcouple sandwich
a bare foil thermocouple was used to measure the sample
temperature. This resulted in a frequent short circuit
between the electrically conductive surface of the glass
slide and the thermocouple wires when moisture condenses
on the cryostage during freezing. To solve this problem
insulated (teflon coated) thermocouple wires were used.

Finally to minimize the disturbance that results
from condensation on the crysostage during freezing, a
plastic condensation box was built around the microscope.
The box has inlet and outlet parts which are used for
flushing with dry nitrogen gas prior to an experimental run.

The box proved to be an efficient way for minimizing the condensation, however it did not prevent condensation completely.

APPENDIX C

APPENDIX C

Statistical Calculations

1) Membrane Water Permeability L_p as a Function of Solute Concentration:

To justify the dependence of L_p on the external solute concentration, the slope of the regression line in Figure 19 was tested statistically. Chapter 12 of reference 61 details the required procedure.

The following values were determined from the experimental data in order to determine the confidence limits for the slope of regression line.

$n = 18$ (number at points)

$\Sigma x_i = 38.13$

$\Sigma y_i = 14.41$

$\Sigma x_i y_i = 29.64$

$\Sigma x_i^2 = 86.31$

$\Sigma y_i^2 = 11.74$

$\bar{x} = 2.12$

$y = 0.8$

The slope (b) and the y intercept (a) of the least squares line $y = bx + a$ are obtained using the following two expressions:

$$b = \frac{n\Sigma x_i y_i - (\Sigma x_i)(\Sigma y_i)}{n\Sigma x_i^2 - (\Sigma x_i)^2}$$

$$a = \bar{y} - b\bar{x}$$

Solving the equations yields

$$a = 1.14$$

$$b = -0.159$$

In order to calculate whether the slope of -0.159 is significantly different than zero the following quantities must be calculated.

$$S_{xx} = n\Sigma x_i^2 - (\Sigma x_i)^2 = 99.9$$

$$S_{yy} = n\Sigma y_i^2 - (\Sigma y_i)^2 = 3.78$$

$$S_{xy} = n\Sigma x_i y_i - (\Sigma x_i)(\Sigma y_i) = -15.89$$

$$S_e = \left[\frac{S_{xx} S_{xy} - (S_{xy})^2}{n(n-2)(S_{xx})} \right]^{1/2} = 0.066$$

The confidence limits for the slope b are

$$b \pm (t_{\alpha/2})(S_e)\sqrt{n/S_{xx}}$$

At the 99% confidence lvel for 16 degrees of freedom

$$t_{\alpha/2} = 2.921$$

which yields

$$-0.22 \leq \beta \leq -0.1$$

This interval does not include the zero. Hence we can conclude that at the 99% confidence level the slope b is different than zero. A test of this hypothesis is performed in order to assess the validity of the above conclusion. The null hypothesis to be tested is H_0: $\beta = 0$ and the appropriate alternative is H_1: $\beta \neq 0$. Using the equation

$$t = \frac{(b - \beta_o)}{S_e} \sqrt{\frac{\overline{S_{xx}}}{n}}$$

yields

$$t = 5.675$$

and since this exceeds 2.921, the value for $t_{\alpha/2}$, we can reject the null hypothesis at the 0.01 level of significance. In other words, we can conclude that there is a relationship between L_p and the solute concentration.

2) Nucleation Temperature as a Function of Cooling
    Rate for Unprotected Hamster Ova:

Following the example given above the following
values were calculated for the experimental data obtained
for nucleation temperatures as a function of cooling
rate:

$b = 0.107$

$S_{xx} = 13196$

$S_{yy} = 5438.24$

$S_{xy} = 1416.8$

$S_e = 1.506$

$t_{0.005} = 2.576$ (at 99% level of confidence)

Then the value of the estimator β is

$-0.078 \leqslant \beta \leqslant 0.292$

Threfore, the value of zero slope is included in the
limits, and we can conclude that at the 99% level of
confidence the nucleation temperature is independent of
the cooling rate.

LIST OF REFERENCES

LIST OF REFERENCES

1. Polge, C., Smith, A.U. and Parkes, A.S., "Revival of Spermatozoa after Vitrification and Dehydration at Low Temperatures," Nature 164, 666 (1949).

2. Lovelock, J.E., "The Denaturation of Lipid-Protein Complex as a Cause of Damage by Freezing," Proc. Roy. Soc. Ses. B 147, 427-433 (1957).

3. Lovelock, J.E., "The Haemolysis of Human Red Cells by Freezing and Thawing," Biochim. Biophys. Acta 10, 414-426 (1953).

4. Doebler, G.F. and Rinfret, A.P., "The Influence of Protective Compounds and Cooling and Warming Conditions on Hemolysis of Erythrocytes by Freezing and Thawing," Biochim. Biophys. Acta 58, 449-458 (1962).

5. Meryman, H.T., "Modified Model for the Mechanism of Freezing Injury in Erythrocytes," Nature 218, 333-336 (1968).

6. Mazur, P., Leibo, S.P., and Chu, E.H.Y., "A Two-Factor Hypothesis of Freezing Injury-Evidence from Chinese Hamster Tissue Culture Cells," Exp. Cell Res. 71, 345-355 (1972).

7. Mazur, P., Leibo, S.P., Farrant, J., Chu, E.H.Y., Hanna, Jr., M.G., and Smith, L.H., in The Frozen Cells, eds., Wolstenholme, G.E.W. and O'Connor, M., Churchill, London, (1970).

8. McGrath, J.J., "Preservation of Biological Material by Freezing," in Heat Transfer in Medicine and Biology: Analysis and Applications, eds., Ebrhart and Shitzer, (1983).

9. Mazur, P., "The Role of Intracellular Freezing in the Death of Cells Cooled at Supra-Optimal Rates," Cryobiology 14, 251-272 (1977).

10. Silvares, O.M., Cravalho, E.G., Toscano, W.M., and Huggins, C.E., "The Thermodyanmics of Water Transport for Biological Cells During Freezing," Trans. A.S.M.E., J. Heat Transfer 98, 582-588 (1975).

11. Diller, K.R., "A Simple Computer Model for Cell Freezing," Proc. 1977 Super Computer Simulation Conference, Simulation Councils, Inc., La Jolla, CA, 455-459 (1977).

12. Diller, K.R. and Cravalho, E.G., "A Cryomicroscope for the Study of Freezing and Thawing Processes in Biological Cells," Cryobiology 7, 191-199 (1971).

13. Diller, K.R., Cravalho, E.G., and Huggins, C.E., "Intracellular Freezing in Biomaterials," Cryobiology 9, (1972).

14. McGrath, J.J., Cravalho, E.G., and Huggins, C.E., "An Experimental Comparison of Intracellular Ice Formation and Freeze-Thaw Survival of Hela 5-3 Cells," Cryobiology 12, 540-550 (1975).

15. Schwartz, G.J. and Diller, K.R., "Design and Fabrication of a Simple, Versatile Cryomicrosope Stage," Cryobiology 19, 529-538 (1982).

16. Whittingham, D.G., Leibo, S.P., and Mazur, P., "Survival of Mouse Embryos Frozen to -196 and -296°C," Science 178, 411-414 (1972).

17. Whittingham, D.G., "Fertilization *In Vitro* and Development to Term of Unfertilized Mouse Oocytes Previously Stored at -196°C," J. Reprod. Fert. 49, 89-94 (1977).

18. Elliott, K. and Whelan, J., "The Freezing of Mammalian Embryos," Ciba Foundation Symposium 52, Elsevier, Amsterdam (1977).

19. Leibo, S.P., "Water Permeability and Its Activation Energy of Fertilized and Unfertilized Mouse Ova," J. Membrane Biol. 53, 179-188 (1980).

20. Mazur, P., "Kinetics of Water Loss from Cells at Subzero Temperatures and the Likelihood of Intracellular Freezing," J. Gen. Physiol. 47, 347-369 (1963).

21. Levin, R.L., "Kinetics of Water Transport in Biomaterials During Freezing," Ph.D. Thesis, Department of Mechanical Engineering, MIT (1976).

22. Levin, R.L., Cravalho, E.G., and Huggins, C.E., "Effect of Hydration on the Water Content of Human Erythrocytes," Biophys. J. 16, 1411-1426 (1976).

23. Cosman, M.D., "Optimal Cooling Protocols for Cryopreservation of Individual Cells," M.S. Thesis, Department of Mechanical Engineering, MIT (1978).

24. Knox, J.M., Schwartz, G.J., and Diller, K.R., "Volumetric Changes in Cells During Freezing and Thawing," Trans. A.S.M.E., J. Biomech. Engr. 102, 91-97 (1980).

25. Mansoori, G.A., "Kinetics of Water Loss from Cells at Subzero Centigrade Temperatures," Cryobiology 12, 34-45 (1975).

26. Callow, R.A., "Thermodynamic Modelling and Cryomicroscopy of Large Unilamellar Liposomes," M.S. Thesis, Department of Mechanical Engineering, Michigan State University (1983).

27. Castellan, G.W., Physical Chemistry, Addison-Wesley, Reading, MA (1971).

28. Katchalsky, A. and Curran, P.F., Nonequilibrium Thermodynamics in Biophysics, Harvard University Press, Cambridge, MA (1967).

29. Terwilliger, T.C. and Solomon, A.K., "Osmotic Water Permeability of Human Red Cells," J. Gen. Physiol. 77, 549-570 (1981).

30. Levin, R.L., "Water Permeability of Yeast Cells at Sub-Zero Temperatures," J. Membrane Biology 46, 91-124 (1979).

31. Diller, K.R. and Bradley, D.A., "Measurement of the Water Permeability of Single Human Granulocytes on a Microscopie Stopped-Flow Mixing System," J. Biomech. Engr. __, (1983).

32. Scheiwe, M.W., Körber, C., "Basic Investigations on the Freezing of Human Lymphocytes," Cryobiology, in press.

33. Scheiwe, M.W. and Körber, C., "Basic Investigations on the Freezing of Human Leurocytes," Cryobiology, in press.

34. DeMayo, F.J., "Xenogenous Fertilization of Cryo-preserved Golden Hamster and Squirrel Monkey Ova," Ph.D. Thesis, Department of Physiology, Michigan State University (1983).

35. Ligon, R., Michigan State University, personal communication.

36. Nowlen, S.P., "Experimental and Analytical Methods for the Determination of the Permeability Characteristics of Individual Cell Membranes," M.S. Thesis, Michigan State University (1983).

37. Luké, B., and McCutcheon, M., "The Living Cell as an Osmotic System and its Permeability to Water," Physiol. Rev. 12, 68-139 (1932).

38. Morris, G.J. and McGrath, J.J., "Intracellular Ice Nucleation and Gas Bubble Formation in Spirogyra," Cryo-Letters 2, 341-352 (1981).

39. Tu, S.M., "Computer Simulation of Two-Dimensional Transient Temperature Field in Cryomicroscope Conduction Stage," M.S. Thesis, Michigan State University (1983).

40. Diller, K.R., "A Microscopic Investigation of Intracellular Ice Formation in Frozen Human Erythrocytes," Ph.D. Thesis, Department of Mechanical Engineering, MIT (1972).

41. Schwartz, G.J. and Diller, K.R., "Osmotic Response of Individual Cells During Freezing: II. Membrane Permeability Analysis," Cryobiology, (1983), in press.

42. Schwartz, G.J. and Diller, K.R., "Cryomicroscopic Measurement and Interpretation of Transient Granulocyte Volumes During Freezing," Cryobiology submitted.

43. Schwartz, G.J. and Diller, K.R., "Analysis of the Water Permeability of Human Granulocytes at Subzero Temperatures in the Presence of Extracellular Ice," Transactions A.S.M.E., Journal of Biochemical Engineering, submitted.

44. Hempling, H.G., "Heats of Activation for the Exosmotic Flow of Water Across the Membrane of Leukocytes and Leukemic Cells," Joural of Cellular and Comparative Physiology 81, 1-9 (1973).

45. Rich, G.T., Sha'afi, R.I., Romualdez, A., and Solomon, A.R., "Effect of Osmolality on the Hydraulic Permeability Coefficient of Red Cells," J. General Physiol. 52, 941-953 (1968).

46. Papanek, T.H., "The Water Permeability of the Human Erythrocyte in the Temperature Range +25°C to -10°C," Ph.D. Thesis, MIT, Cambridge, MA (1978).

47. Scheiwe, M.W., Körber, C., and Wollhover, K., "A Method of Calculation of Optimal Cooling Rates for Cryopreservation of Blood Cells on the Basis of Volume Loss During Freezing," Cryobiology 18, 625 (1981).

48. Farmer, R.E.L. and Macey, R.I., "Perturbation of Red Cell Volume: Rectification of Osmotic Flow," Biochim. Biophys. Acta 196, 53-65 (1970).

49. Outhred, R. and Colon, T., "The Volume Dependence of the Erythrocyte Water Diffusion Permeability," Biochim. Biophys. Acta 318, 446-450 (1973).

50. Forster, R.E., "The Transport of Water in Erythrocytes," in Current Topics in Membranes and Transport, eds., F. Bronner and A. Kleinzeller, Vol. 2, 42-98, Academic Press, New York (1971).

51. Pushkar, N.S., Itkin, Y.A., Bronsteir, V.L., Gordiyenko, E.A. and Komin, Y.U., "On the Problem of Dehydration and Intracellular Crystallization During Freezing of Cell Suspensions," Cryobiolgoy 13, 147-152 (1976).

52. Levin, R.L., Cravalho, E.G. and Huggins, C.E., "The Concentration Polarization Effect in a Multicomponent Electrolyte Solution—The Human Erythrocytes," J. Theor. Biol. 71, 225-254 (1978).

53. McGrath, J.J., "Thermodynamic Modeling of Membrane Damage," in Effects of Low Temperatures on Biological Membranes, eds., G.J. Morris and A. Clarke, 335-377 Academic Press, New York (1981).

54. Luké, B., Hartline, H.K., and McCutcheon, M., "Further Studies on the Kinetics of Osmosis in Living Cells," J. Gen. Physiol. 14, 405-419, (1931).

55. Levin, R.L., Cravalho, E.G., and Huggins, C.E., "Effect of Solution Non-Ideality on Erythrocyte Volume Regulation," Biochim. Biophys. Acta 465, 179-190 (1977).

56. McCutcheon, M. and Luké, B., "The Effect of Temperature on Permeability to Water of Resting and Activated Cells (Unfertilized and Fertilized Eggs of Arbacia Punctulata)," J. Cell Comp. Physiol. 2, 11 (1932).

57. Asahina, E., "Intracellular Freezing and Frost Resistance in Egg Cells of the Sea Urchin," Nature (London) 191, 1263-1265 (1961).

58. Asahina, E., "Frost Injury in Living Cells," Nature (London) 196, 445-446 (1962).

59. Leibo, S.P., McGrath, J.J., and Cravalho, E.G., "Microscopic Observation of Intracellular Ice Formation in Unfertilized Mouse Ova as a Function of Cooling Rate," Cryobiology 15, 257-271 (1978).

60. Rall, W.F., Mazur, P. and McGrath, J.J., "Depression of the Ice-Nucleation Temperature of Rapidly Cooled Mouse Embryos by Glycerol and Dimethyl Sulfoxide," Biophys. J. 41, 1-12 (1983).

61. Miller, I. and Freund, J.E., "Probability and Statistics for Engineers," Prentice-Hall, Inc., Englewood Cliffs, NJ, (1965).